Proposal to PAC 20 **May 31, 2001**

The Electric Form Factor of the Neutron at $Q^2 = 2.40$ (GeV/c)^2 [and the Proton at $Q^2 = 2.08$ (GeV/c)^2]

Spokesman: R. Madey, Kent State U & Jefferson Lab

Co-Spokesman: S. Kowalski, MIT

Abstract

We propose to extend measurements of the electric form factor of the neutron, G_E^n, to a squared four-momentum transfer of 2.40 (GeV/c)^2. The JLab E93-038 collaboration conducted d($\vec{e}$,e'$\vec{n}$)p measurements on a liquid deuterium target from September 8, 2000, to April 26, 2001 at Q^2 values of 0.45, 1.13, and 1.47 (GeV/c)^2. *Polarization-transfer measurements above $Q^2 \approx$ 1 (GeV/c)^2 are unique to CEBAF and require the neutron polarimeter and the Charybdis neutron spin precession magnet that were used in E93-038 to measure the ratio of two scattering asymmetries associated with plus and minus precessions of the neutron polarization vector.* In this ratio technique, systematic uncertainties are small because the analyzing power of the polarimeter cancels in the ratio, and the beam polarization cancels also because, as demonstrated in E93-038, the beam polarization does not change much in sequential measurements of the two scattering asymmetries. The primary motivation for this measurement is the unique ability to measure a fundamental quantity of the neutron — one of the basic building blocks of matter.

Also we propose to measure g_p [$\equiv G_E^p/G_M^p$] by another independent polarization-transfer technique for the purpose of determining if there is a fundamental problem with either the Rosenbluth or focal-plane polarimeter (FPP) methods. Our proposed measurement of G_E^p would be incidental to the G_E^n measurement. With a relatively small investment of time, the g_p measurement at $Q^2 = 2.08$ (GeV/c)^2 is designed to distinguish clearly between $\mu_p g_p = 0.73$ from JLab E93-027 and $\mu_p g_p \approx 1$ from the SLAC global analysis. *The method proposed here with a dipole precession magnet and a stand-alone proton polarimeter has the advantage over the FPP method that the precession of the polarization vector is easy to calculate and practically no error can occur.*

List of Participants

R. Madey (Spokesman), B.D. Anderson (Institutional Representative), A.R. Baldwin, D.M. Manley, A.Yu. Semenov, W. Tireman, J.W. Watson, W.-M. Zhang, C. Yan

Kent State University

R. Carlini (*Institutional Representative*), R. Ent, H. Fenker, K. Garrow, M. Jones, A. Lung, D. Mack, G. Smith, W. Vulcan, S. Wood, C. Yan

Thomas Jefferson National Accelerator Facility

S. Kowalski (Co-Spokesman and Institutional Representative), M. Farkhondeh, B. Plaster, S. Taylor

Massachusetts Institute of Technology

S. Churchwell, C. Howell (*Institutional Representative*), S. Tajima

Duke University

H. Breuer, J.J. Kelly (*Institutional Representative*), N. Savvinov

University of Maryland

E. Crouse, J.M. Finn (*Institutional Representative*), F. Gross, C. Perdrisat

The College of William and Mary

O.K. Baker (*Institutional Representative*), E. Christy, L. Cole, L. Gan, A. Gasparian, P. Gueye, B. Hu, C. Keppel, L. Tang, L. Yuan

Hampton University

A. Ahmidouch (*Institutional Representative*), S. Danagoulian,

North Carolina A&T State University

G. MacLachlan, A. Opper (*Institutional Representative*)

Ohio University

List of Participants (continued)

A. Aghalaryan, R. Asaturyan, H.G. Mkrtchyan (*Institutional Representative*), S. Stepanyan, V. Tadevosyan,

Yerevan Physics Institute

S. Wells (*Institutional Representative*), N. Simicevic

Lousisiana Tech

P. Markowitz (*Institutional Representative*), B. Raue, J. Reinhold

Florida International University

D. Day (*Institutional Representative*), F. Wesselmann, H. Zhu

University of Virginia

P. Ulmer

Old Dominion University

M. Khandaker (*Institutional Representative*), V. Punjabi

Norfolk State University

M. Elaasar

Southern University at New Orleans

R.E. Segel

Northwestern University

R. Wilson

Harvard University

W.-Y. Kim (*Institutional Representative*), W. Seo

Kyungpook National University

T. Reichelt

University of Bonn

H. Arenhovel

University of Mainz

Contents

List of Figures

List of Tables

1 Scientific Motivation and Background

1.1 Extension of E93-038 to Measure G_E^n at $Q^2 = 2.40$ (GeV/c)^2

The electric form factor G_E^n of the neutron is a fundamental quantity needed for the understanding of both nucleon and nuclear structure. The dependence of G_E^n on Q^2 is determined by the distribution of charge in the neutron. The E93-038 collaboration carried out measurements of G_E^n from September 8, 2000 to 26 April 2001 at three values of Q^2 [viz., 0.45, 1.13, and 1.47 (GeV/c)^2], the squared four-momentum transfer. Figure 1 is a plot G_E^n vs Q^2 of the world data from polarization-transfer measurements. Very preliminary results [**not for quotation**] of an early analysis of some of the data from E93-038 indicate that G_E^n follows the parameterization of Galster et al. (1971). The Galster parameterization is plotted as a solid line in Fig. 1. Based on the data collected in E93-038, the uncertainties expected after completion of the data analysis are plotted as blue squares on the axis $G_E^n = 0$. Also plotted in Fig. 1 are world data on G_E^n from polarization-transfer measurements. Literature references to these data include Eden et al. (1994), Meyerhoff et al. (1994), Schmieden (1996), Klein and Schmieden (1997a), Klein (1997b), Ostrick et al. (1999), Herberg et al. (1999), Passchier et al. (1999), Rohe et al. (1999), and Zhu et al. (2001).

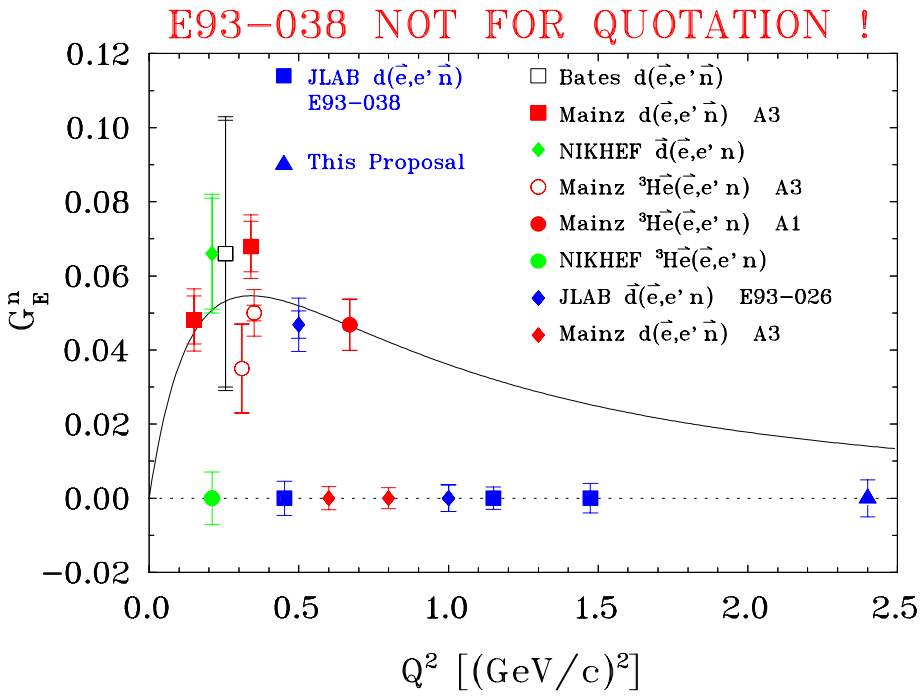

Figure 1: G_E^n vs Q^2. The line reflects the Galster parameterization of G_E^n. The statistical uncertainties expected in E93-038 after completion of the data analysis are plotted on the axis $G_E^n = 0$.

Polarization-transfer measurements at Q^2 above ≈ 1 (GeV/c)^2 are unique to CEBAF, and also to the technique demonstrated in E93-038 with a high-efficiency polarimeter and a dipole magnet ahead of the polarimeter to precess the spin of the neutron. In this technique, we measure the ratio of two neutron scattering asymmetries: one asymmetry from precessing the neutron

polarization vector in a positive direction; the other, from precessing in a negative direction. In this ratio technique, systematic uncertainties are small because the analyzing power cancels in the ratio, and the beam polarization cancels also because, as demonstrated in E93-038, the beam polarization does not change much during the sequential measurements of the scattering asymmetries.

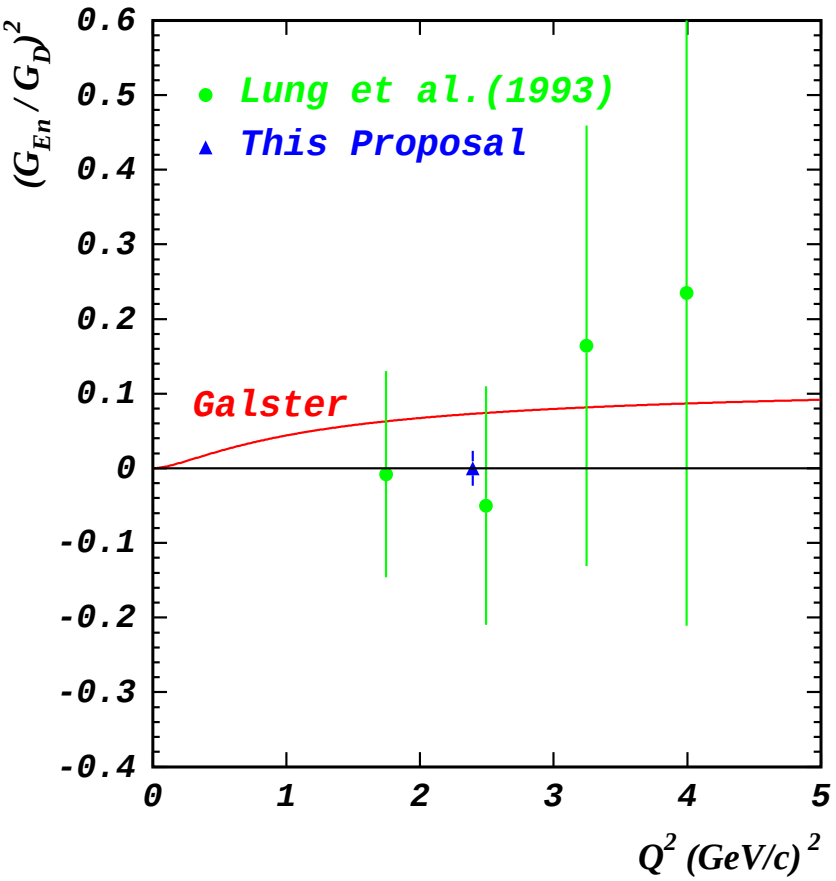

Figure 2: $(G_E^n/G_D)^2$ as a function of Q^2. The data are from SLAC-NE11 [Lung et al. (1993)]. The solid line is the Galster parameterization. The uncertainty projected in this proposal for $Q^2 = 2.40$ (GeV/c)^2 is for a value $(G_E^n/G_D)^2 = 0.0365$, which is one-half of the Galster value.

In the high Q^2 region above 1.5 (GeV/c)^2, our present knowledge of the electric and magnetic form factors G_E and G_M for neutrons was obtained from measurements of the angular dependence of the cross section by quasielastic electron-deuteron scattering. Subtraction of the contribution from the proton in the deuteron introduces a large uncertainty. These previous experiments contain large systematic errors because of uncertainties in the theoretical description of the deuteron, mostly from final-state interactions (FSI) and meson-exchange currents (MEC). In the Q^2 region from 1.75 to 4 (GeV/c)^2, Lung et al. (1993) reported measurements from SLAC-NE11 of quasielastic e-d cross sections at forward and backward angles, which permit Rosenbluth separation of G_E^n and G_M^n at $Q^2 = 1.75$, 2.50, 3.25, and 4.00 (GeV/c)^2. The data of Lung et al. (1993) for $(G_E^n/G_D)^2$ are plotted in Fig. 2 as a function of Q^2. Also plotted in Fig. 2 is the Galster parameterization. The error bars from JLab E93-038 will be much

smaller than those from SLAC-NE11. Although Lung et al. (1993) stated that their G_E^n data from SLAC-NE11 were consistent with $(G_E^n)^2 = 0$ for 1.75< Q^2 (GeV/c)^2 <4.00, these data appear consistent also with the Galster parameterization. The NE11 error bars do not permit distinguishing between $(G_E^n)^2 = 0$ and the Galster parameterization. *The correct Q^2-dependence of G_E^n above 1.5 (GeV/c)^2 remains in doubt.* We need to know whether G_E^n will continue to follow the Galster parameterization above Q^2 = 1.5 (GeV/c)^2, or whether G_E^n will approach zero or even become negative. There is no theoretical reason for G_E^n to follow the Galster parameterization at high Q^2 values. The parameterization of Galster et al. (1971) for G_E^n was based on the best fit to the experimental data available on electron-deuteron scattering up to Q^2 = 1.0 (GeV/c)^2. The best fit was found with the wave function of Feshbach and Lomon (1967). Our technique permits us to extend the measurements of G_E^n to the Q^2 region up to about 2.5 (GeV/c)^2. *In contrast to the Rosenbluth separation method, the polarization transfer method proposed here permits an experimental determination of the sign of G_E^n. This ability is another nice feature of the polarization transfer technique — especially in view of the fact that nothing is known about the sign of G_E^n at high Q^2.* Here we propose to measure G_E^n at Q^2 = 2.4 (GeV/c)^2 with sufficient accuracy to challenge rigorous Lattice QCD calculations.

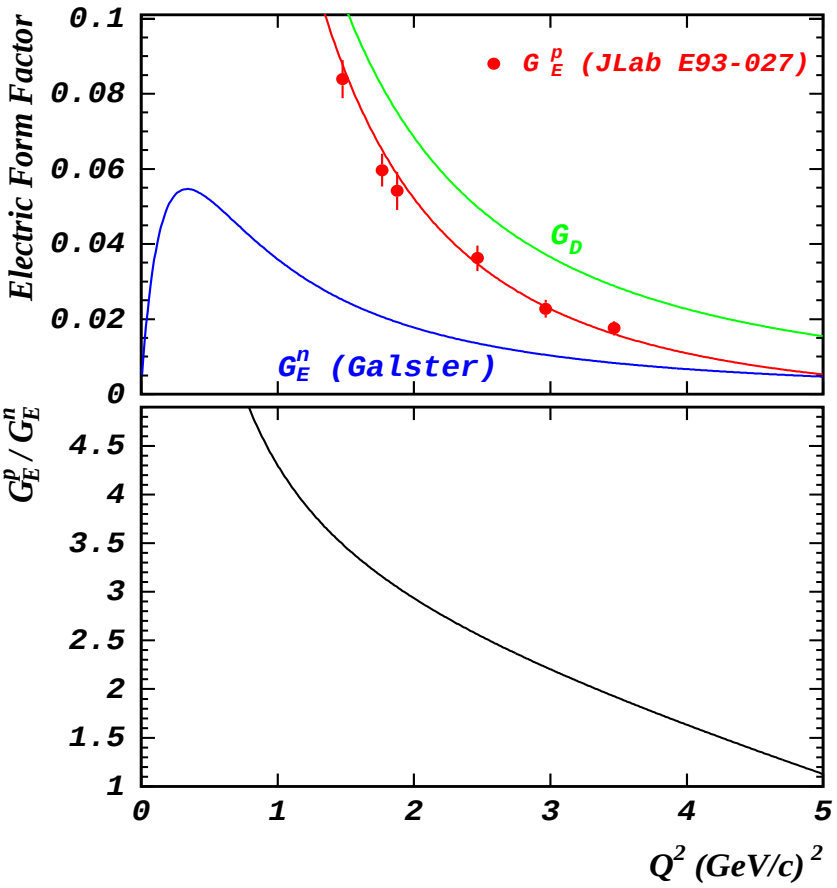

Figure 3: Proton and neutron form factors as a function of Q^2. Red solid line in the top panel is a parameterization from Eq. (4) for G_E^p.

As Q^2 increases, the values of G_E^p, the elastic form factor of the proton, approach the values

of G_E^n, represented by the Galster parameterization. Plotted in Fig. 3 as a function of Q^2 are the neutron electric form factor for the Galster parameterization, the proton electric form factor for the dipole parameterization, and the proton electric form factor points measured in JLab E93-027. The Galster parameterization for G_E^n is:

$$G_E^n = -\tau(1+5.6\tau)^{-1}G_M^n \qquad (Galster) \tag{1}$$

with

$$G_M^n = 1.91(1+Q^2/0.71)^{-2} \qquad (Dipole) \tag{2}$$

$$\tau = Q^2/4M^2 \tag{3}$$

The measured G_E^p points have been fitted with the following parameterization:

$$G_E^p = G_D\,[1-0.14(Q^2-0.30)] \quad (Fit\ \ to\ \ Hall\ A\ \ FPP\ \ Measurements) \tag{4}$$

with

$$G_D \ \equiv \ (1+Q^2/0.71)^{-2} \qquad (Dipole) \tag{5}$$

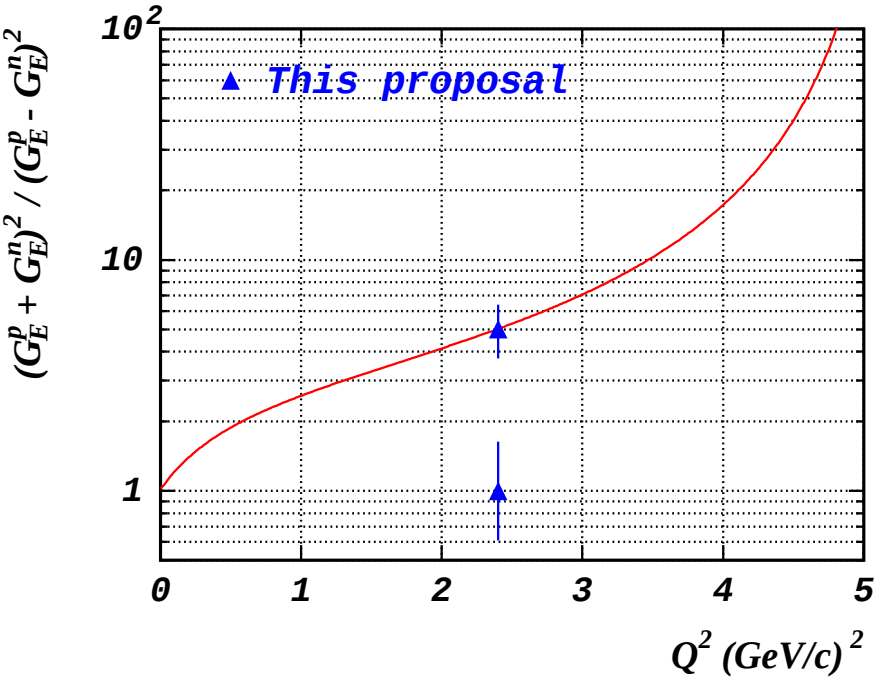

Figure 4: The ratio of isoscalar and isovector cross-sections [Eq. (6)] as a function of Q^2. We assume the Galster parameterization for G_E^n [Eq. (1)] and the parameterization from Eq. (4) for G_E^p. The error bars for presented points originate from projected uncertainty $\Delta G_E^n = 0.0045$ and uncertainty of E93-027 measurement at $Q^2 = 2.47$ (GeV/c)^2 ($\mu_p g_p = 0.726 \pm 0.027 \pm 0.062$).

The magnitude of G_E^n is not insignificant compared to G_E^p in the Q^2 region above about 2 (GeV/c)^2. The ratio of G_E^p (E93-027) to G_E^n (Galster) is plotted in the bottom panel of Fig. 3.

The G_E^p data measured in E93-037 turned out to be a *surprise* – falling faster with Q^2 than expected from the global analysis of earlier SLAC data (see Fig. 22 ahead). The nature of the decrease of G_E^n with Q^2 may be a surprise also.

Because the isovector electric form factors of nuclei are proportional to the difference $G_E^p - G_E^n$ (and the isoscalar electric form factors are proportional to the sum $G_E^p + G_E^n$), the value of G_E^n is needed for the understanding of electron scattering experiments that probe electric structure functions at high momentum transfer. The ratio of the isoscalar cross section to the isovector cross section depends sensitively on the value of G_E^n.

$$\frac{\sigma_{isoscalar}}{\sigma_{isovector}} = \left(\frac{G_E^p + G_E^n}{G_E^p - G_E^n} \right)^2 \tag{6}$$

This ratio is plotted in Fig. 4 as a function of Q^2. This ratio is unity if $G_E^n = 0$; and this ratio is about five at $Q^2 = 2.4$ (GeV/c)^2 if G_E^n continues to follow the Galster parameterization and if G_E^p follows Eq. (4). A better knowledge of G_E^n is needed for the interpretation of electron scattering from nuclei at high momentum transfer. With an uncertainty $\Delta G_E^n = 0.0045$, we will be able to distinguish between $G_E^n = 0$ and Galster [$G_E^n = 0.014$ at $Q^2 = 2.4$ (GeV/c)^2], and also the proposed datum should help to discriminate between predictions from some of the recent QCD-inspired models.

1.2 Theoretical Background

Arenhoevel (1987) calculated the effect of the electric form factor of the neutron G_E^n on the polarization transfer in the d($\vec{e}$,e'$\vec{n}$)p reaction in the quasifree region, where the deuteron serves as a neutron target while the proton acts mainly as a spectator. Using a nonrelativistic theory and a realistic nucleon-nucleon potential, Arenhoevel found that the sideways polarization of the recoil neutron $P_{S'}$, which vanishes for coplanar kinematics and unpolarized electrons, is most sensitive to G_E^n for neutron emission along the momentum-transfer direction in the quasifree case. Using the parameterization of Galster et al. (1971) for G_E^n, Arenhoevel's calculation indicates that even away from the forward-emission direction (with respect to the direction of the momentum transfer $\vec{q}$), the increase in the sideways polarization of the neutron $P_{S'}$ is small for $G_E^n = 0$, but increases when G_E^n is switched on, and that this increase prevails up to a neutron angle of nearly 30^o measured with respect to $\vec{q}^{\,c.m.}$ in the center-of-mass system. In the forward direction with respect to $\vec{q}^{\,c.m.}$, Arenhoevel found also that the neutron polarization $P_{S'}$ is insensitive to the influence of final-state interactions (FSI), meson-exchange currents, and isobar configurations, and that this lack of sensitivity holds again up to an angle of nearly 20^o away from the forward direction with respect to $\vec{q}^{\,c.m.}$, which corresponds to a laboratory angle of about a few degrees away from the forward direction with respect to the $\vec{q}^{\,lab}$. Also Arenhoevel studied the influence of different deuteron wave functions on the sideways neutron polarization $P_{S'}$. His results for quasifree kinematics (i.e., for neutron emission along $\vec{q}$) show almost no dependence on the deuteron model. The Arenhoevel calculation shows that dynamical uncertainties are very small. Finally, Beck and Arenhoevel (1992) investigated the role of relativistic effects in electrodisintegration of the deuteron for quasifree kinematics. They find that the dependence on the parameterization of the nucleon current in terms of Dirac-Pauli or Sachs form factors is reduced considerably by inclusion of the relativistic contributions.

Rekalo, Gakh, and Rekalo (1989) used the relativistic impulse approximation to describe the polarization effects sensitive to G_E^n in deuteron electrodisintegration. In the deuteron quasielastic peak, the neutron polarizations calculated in the relativistic approach agree with the results of Arenhoevel (1987). A later study by Mosconi, Pauschenwein, and Ricci (1991) of nucleonic and pionic relativistic corrections in deuteron electrodisintegration does not change the results of Arenhoevel. Laget (1990) investigated the effects of nucleon rescatterings and meson-exchange currents on the determination of the neutron electric form factor in the d($\vec{e}$,e'$\vec{n}$)p reaction. He concluded that the measurements of the sideways polarization of the neutron appears to be the most direct way to determine the neutron electric form factor. He concluded also that in quasifree (colinear) kinematics, the neutron polarization in the exclusive reaction is equal to the value expected in the elementary reaction $n(\vec{e},e')\vec{n}$; in contrast, Laget concluded further that corrections from final-state interactions and meson-exchange currents are negligible above Q^2 = 0.30 (GeV/c)^2, but that these corrections become sizeable below this momentum transfer; however, Herberg et al. (1999) found that (even in the quasifree peak) corrections for FSI in d($\vec{e}$,e'$\vec{n}$)p measurements at Mainz amounted to (8±3)% for Q^2 = 0.34 (GeV/c)^2 and (65±3)% for Q^2 = 0.15 (GeV/c)^2 of the value unperturbed by FSI. These corrections were based on the model of Arenhoevel et al. (1988). This correction is needed to account for the two-step process d($\vec{e}$,e'$\vec{p}$)n + d($\vec{p}$,$\vec{n}$) in the deuterium nucleus. In the second charge-exchange step, the sign of the polarization trasferred to the neutron will be opposite to that from the primary d($\vec{e}$,e'$\vec{n}$)p process because sign of the magnetic moment of the proton is opposite to that of the neutron. This effect increases as the p-n charge exchange cross section increases in going to low Q^2.

Gari and Krumpelmann (1992) reanalyzed the electromagnetic form factor data of the nucleon with emphasis on the neutron electric form factor. They showed that strange quark contributions can reduce the neutron electric form factor at low Q^2 with little effect on the other nucleon form factors.

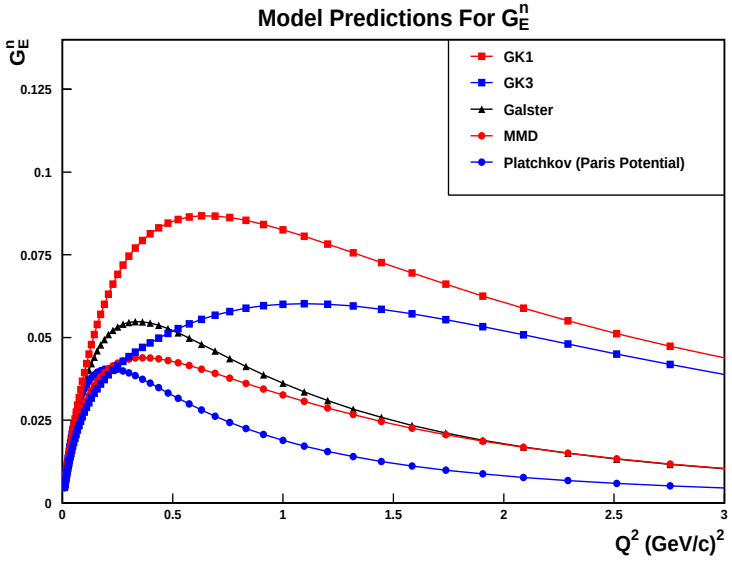

Figure 5: Some model predictions for G_E^n (see text).

Some model predictions for G_E^n are shown in Fig. 5. Existing data [below ≈ 0.7 (GeV/c)^2]

reject the Gari-Krumpelmann (1985) model GK1. Our data from E93-038 will reject another Gari-Krumpelmann (1992) model GK3 and the Platchkov (1990) parameterization with the Paris potential. The model of Mergell, Meissner, and Drechsel (MMD) (1996) gives a result similar to Galster above $Q^2 \approx 0.7$ (GeV/c)^2; but it falls below Galster in the Q^2 region around the peak.

Isgur (1998) noted that the interpretation of the neutron's electric form factor within many models has been obscured by relativistic effects. He demonstrated that, to leading order in the relativistic expansion of a constituent quark model, the Foldy term cancels exactly against a contribution to the Dirac form factor F_1 to leave intact the naive interpretation of G_E^n as arising from the neutron's rest frame charge distribution.

Any model based on Quantum Chromodynamics (QCD) must be able to predict nucleon and pion form factors correctly. QCD models that are used to calculate nucleon form factors include the following: The relativistic constituent quark model [RCQM][Chung and Coester (1991), Aznaurian (1993), Frank, Jennings, and Miller (1996)], the di-quark model [Kroll, Schurmann, and Schweiger (1992)], QCD sum rules [Radyushkin (1984)], and the cloudy bag model [Lu, Thomas, and Williams (1998)]. Recent results from JLab E93-027 on G_E^p motivated RCQM calculations [Pace et al. (2000), De Sanctis et al. (2000), Cardarelli and Simula (2000)]. These recent RCQM calculations reproduce the data of E93-027 when relativistic effects, which were omitted from previous calculations, are included.

Holzwarth (1996) found that a soliton model could reproduce the essential features of nucleon form factors over three orders of magnitude in Q^2. The three basic ingredients in the soliton model of Holzwarth are: (1) an extended object (the standard skyrmion), (2) partial coupling to vector mesons in both isospin channels, and (3) relativistic recoil corrections. The soliton model of Holzwarth describes the G_E^p data from JLab E93-027 and E99-007. The shape of the G_E^n curve (in Fig. 2 of the article by Holzwarth) is similar to the Galster parameterization, but the absolute values of G_E^n are higher by less than a factor of two. Holzwarth states that the absolute values can be reduced by allowing the adjustable parameter λ in the model to differ slightly for isoscalar and isovector mesons.

Isgur and Negele (2000) are leading a major effort to use lattice QCD to understand the structure and interaction of hadrons. Fundamental lattice calculations will be available soon to solve QCD, the field theory of quarks and gluons. Currently lattice calculations are limited by computer power; however, more computing power is expected to be available soon. Lattice QCD calculations are fundamental, whereas various model calculations are not. Lattice QCD has made impressive strides recently, with rigorous methods for separating hard and soft contributions and recent methods for extrapolation to the chiral limit for light quarks using explicit representations of nonanalytic contributions.

Dong et al. (1998) and Liu (2001) reported a lattice QCD calculation of G_E^n in connection with their investigation of the strangeness magnetic moment of the nucleon. The results [from Fig. 5(b) of Dong et al. (1998)] are compared to the Galster parameterization in Fig. 6. Liu (2001) states that the errors are getting too big to made a useful prediction above $Q^2 \approx 1.3$ (GeV/c)^2. Liu (2001) states that the next generation of calculations may reach $Q^2 = 2.4$ (GeV/c)^2. Dong et al. (1998) state that future calculations are needed to investigate the systematic errors associated with the finite volume and lattice spacing as well as with the quenched approximation.

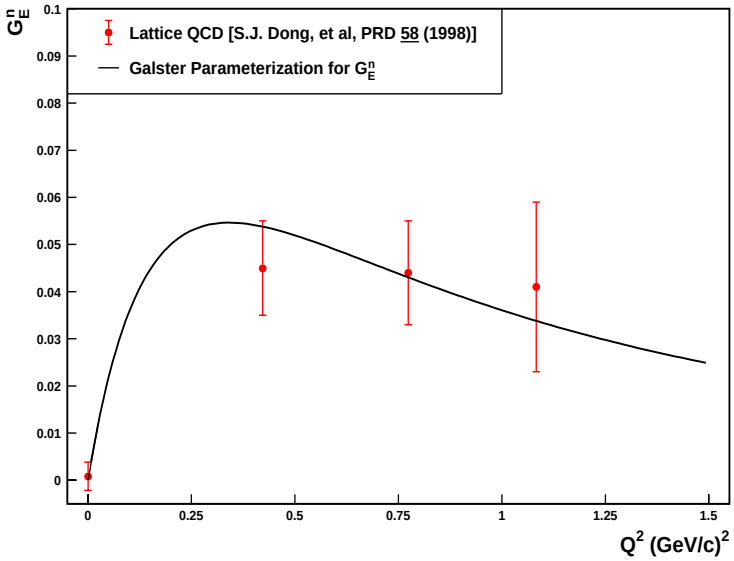

Figure 6: Lattice QCD calculation result for G_E^n.

1.3 Some Results from E93-038

The purpose of this section is to indicate the quality of the data obtained in E93-038. The results shown here for the highest Q^2 [viz., $Q^2 = 1.47$ (GeV/c)^2] are based on an initial analysis of a limited sample of the runs. The top panel in Fig. 7 is an HMS-NPOL coincidence time-of-flight (cTOF) spectrum for all events generated by a neutron incident on the polarimeter. [The reader may wish to look ahead to the Experimental Arrangement Section 2.1.] The incident neutron may scatter elastically to a detector in the rear array or it may cause a proton to be detected in the rear array. The FWHM of the ctof spectrum is about 1.5 ns, and the reals-to-accidentals ratio is ≈ 12 at a beam current of ≈ 60 μA. The bottom panel in Fig. 7 is the TOF spectrum between a neutron event in the front array of the polarimeter and an event in the rear array for both helicity states of the beam. It is called a ΔTOF or dTOF spectrum. The dTOF spectrum can be subdivided into four spectra – two for each beam helicity state (L and R) with scattering to the upper (U) array or to the bottom (D) array; these four dTOF spectra (LU, LD, RU, and RD) appear in Fig. 8. The cross ratio and the asymmetry are calculated from these spectra. A preliminary analysis of the asymmetries for each run and the error-bar weighted average for these data appear in Fig. 9. Correlation between cTOF and dTOF is shown in Fig. 10. This correlation at $Q^2 = 1.13$ (GeV/c)^2 was obtained with the following cuts: (1) a mean-time window duration of 20 ns for both front and rear taggers, and (2) a radius of 30 cm around a neutron track must be free of a charged particle. Application of these cuts is possible only after time calibration procedures, as described by Kelly (2001). Figure 11 illustrates the importance of time calibration also. This figure presents event rates measured in E93-038 at different beam currents. The deviation from plain proportionality between the event rate and the beam current is caused by corruption of electron-neutron coincidence events from accidental background particles (charged or neutral) that appear during the coincidence time window. The fraction of corrupted events (CF) at a certain beam current I can be calculated (see Fig. 24

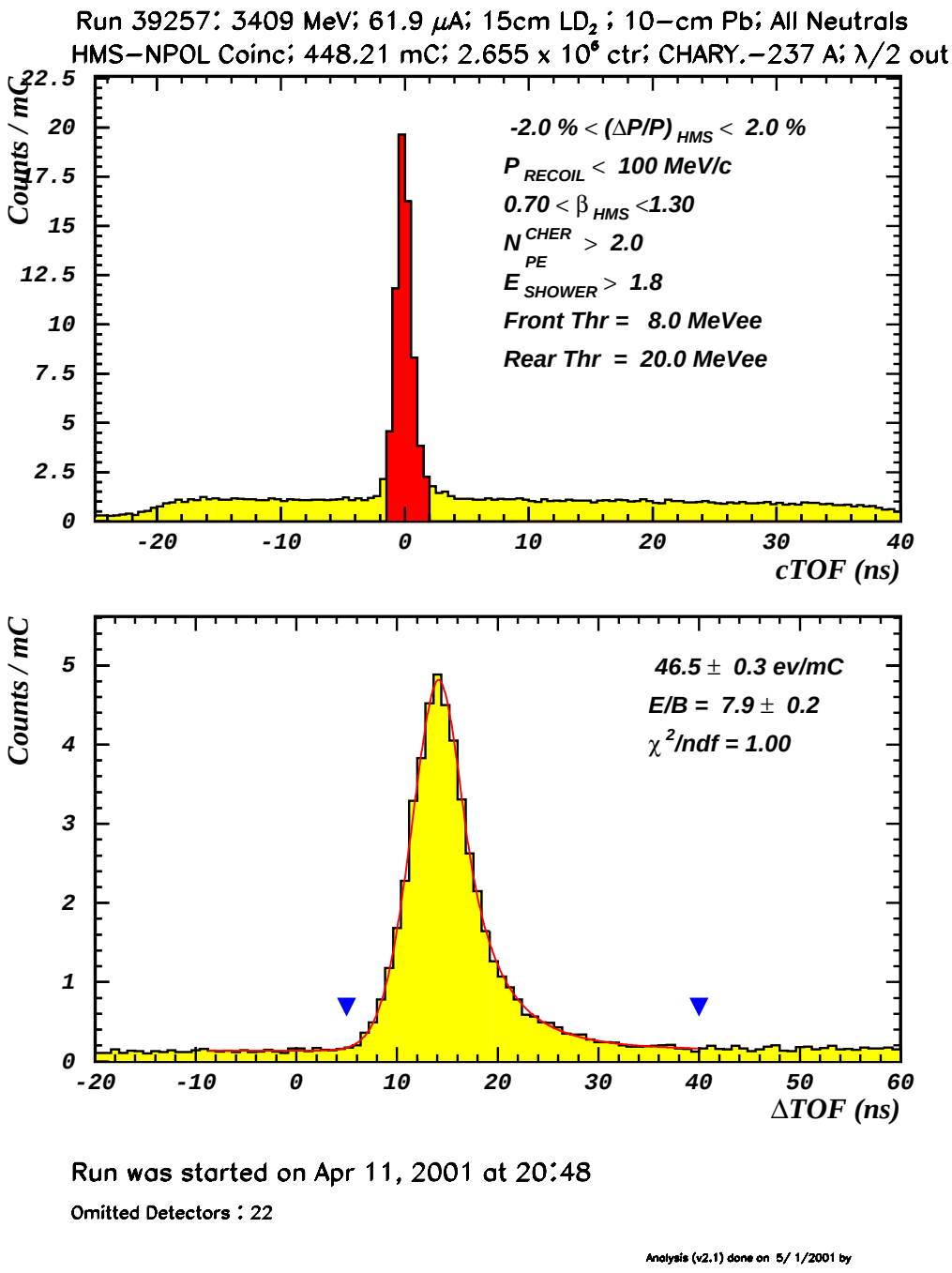

Figure 7: cTOF (top panel) and dTOF (bottom panel) spectra for run 39257 at Q^2 = 1.47 (GeV/c)^2.

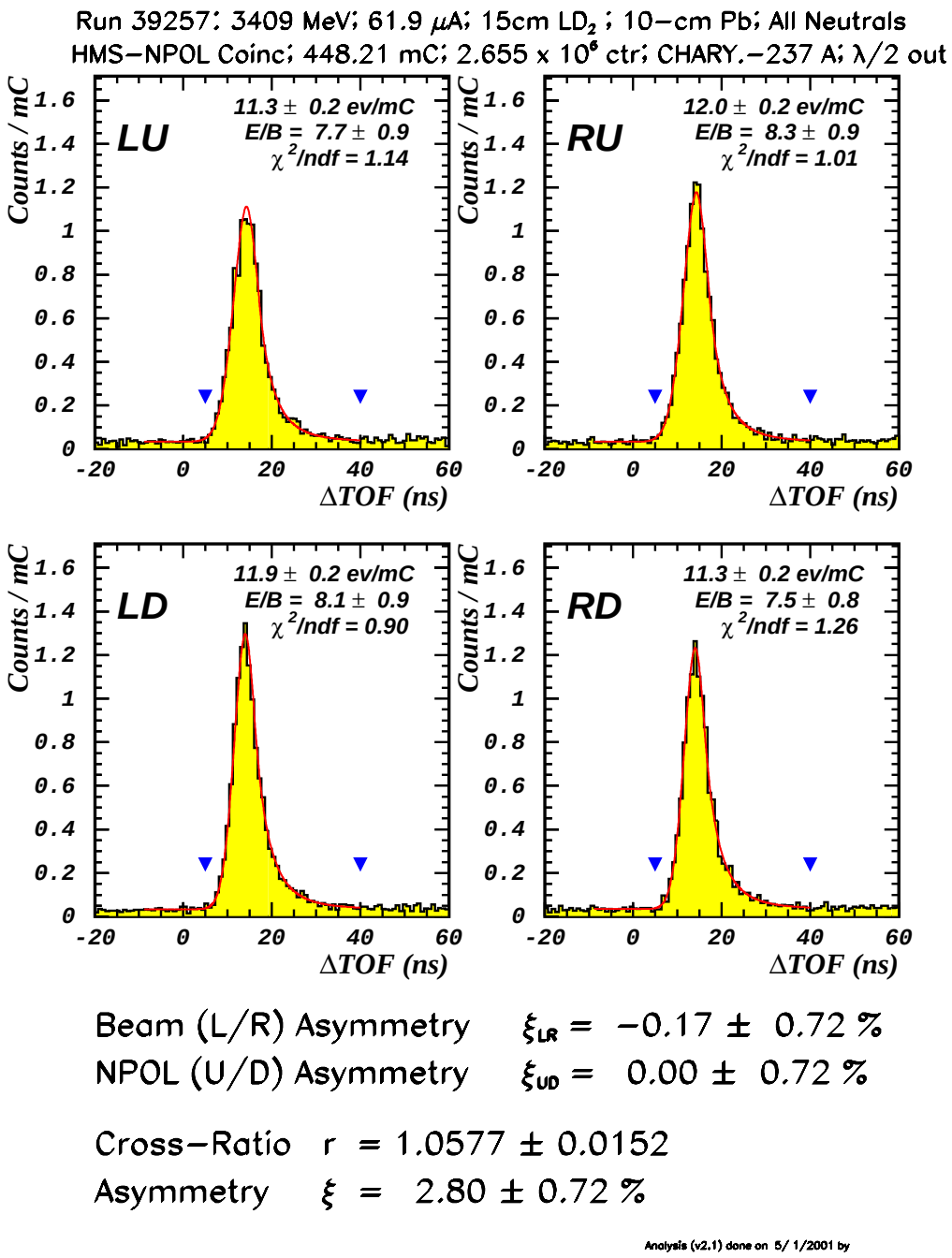

Figure 8: Four dTOF spectra (LU, LD, RU, and RD – see text) for run 39257 at Q^2 = 1.47 (GeV/c)^2.

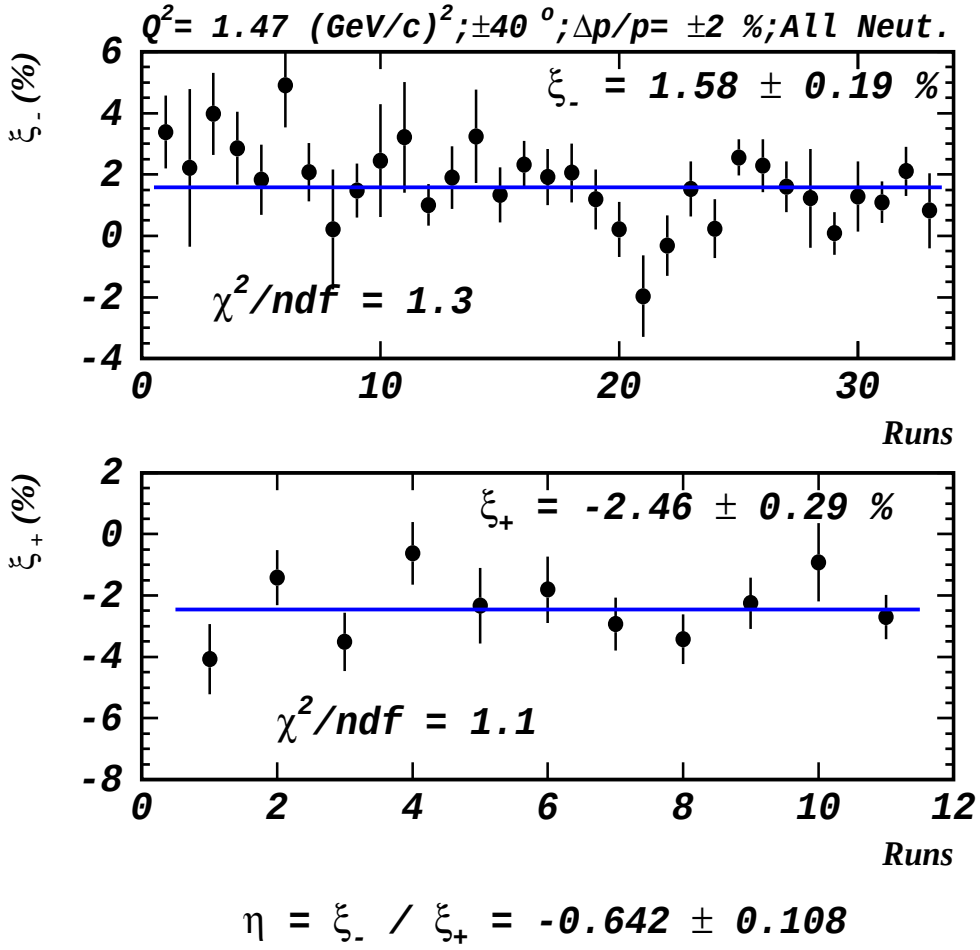

Figure 9: Asymmetries obtained from preliminary analysis of a data sample at $Q^2 = 1.47$ $(\mathrm{GeV/c})^2$ (**not for quotation!**).

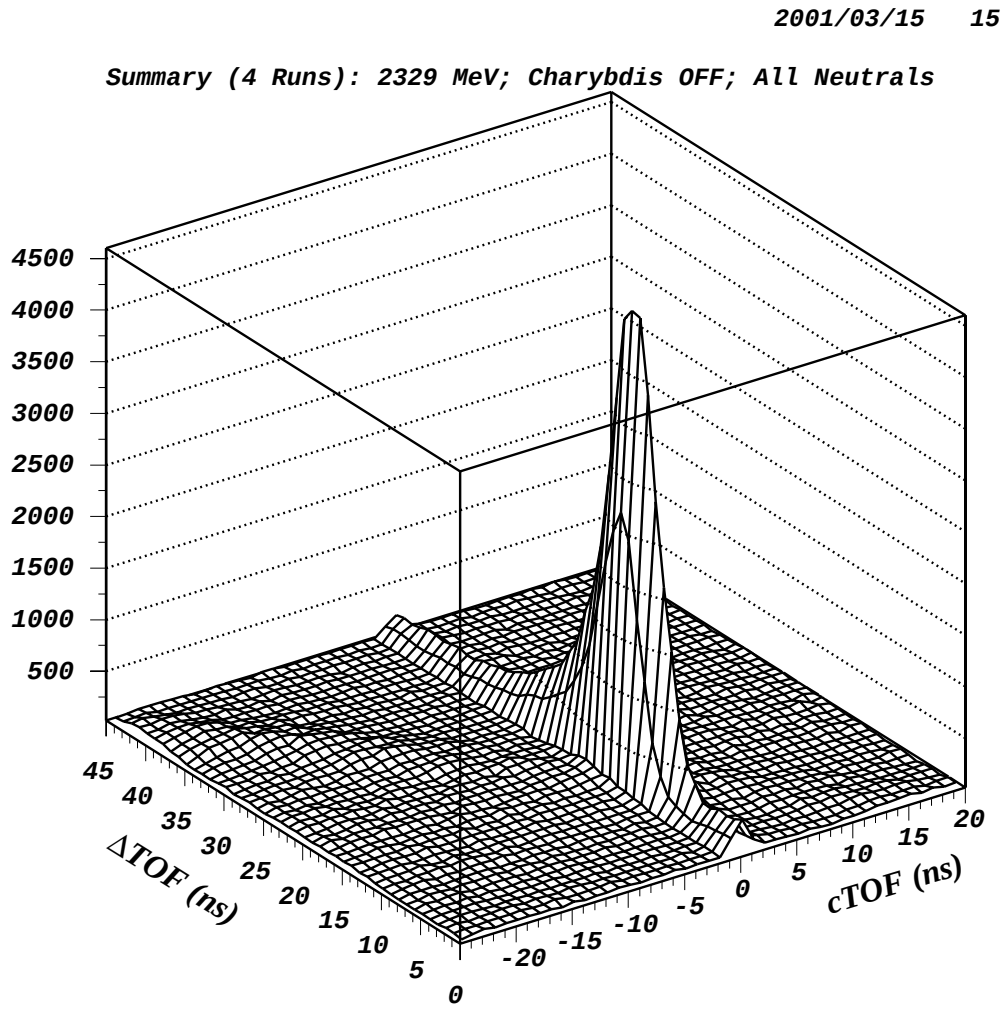

Figure 10: Correlation between cTOF and dTOF for summary of four runs at $Q^2 = 1.13$ (GeV/c)^2.

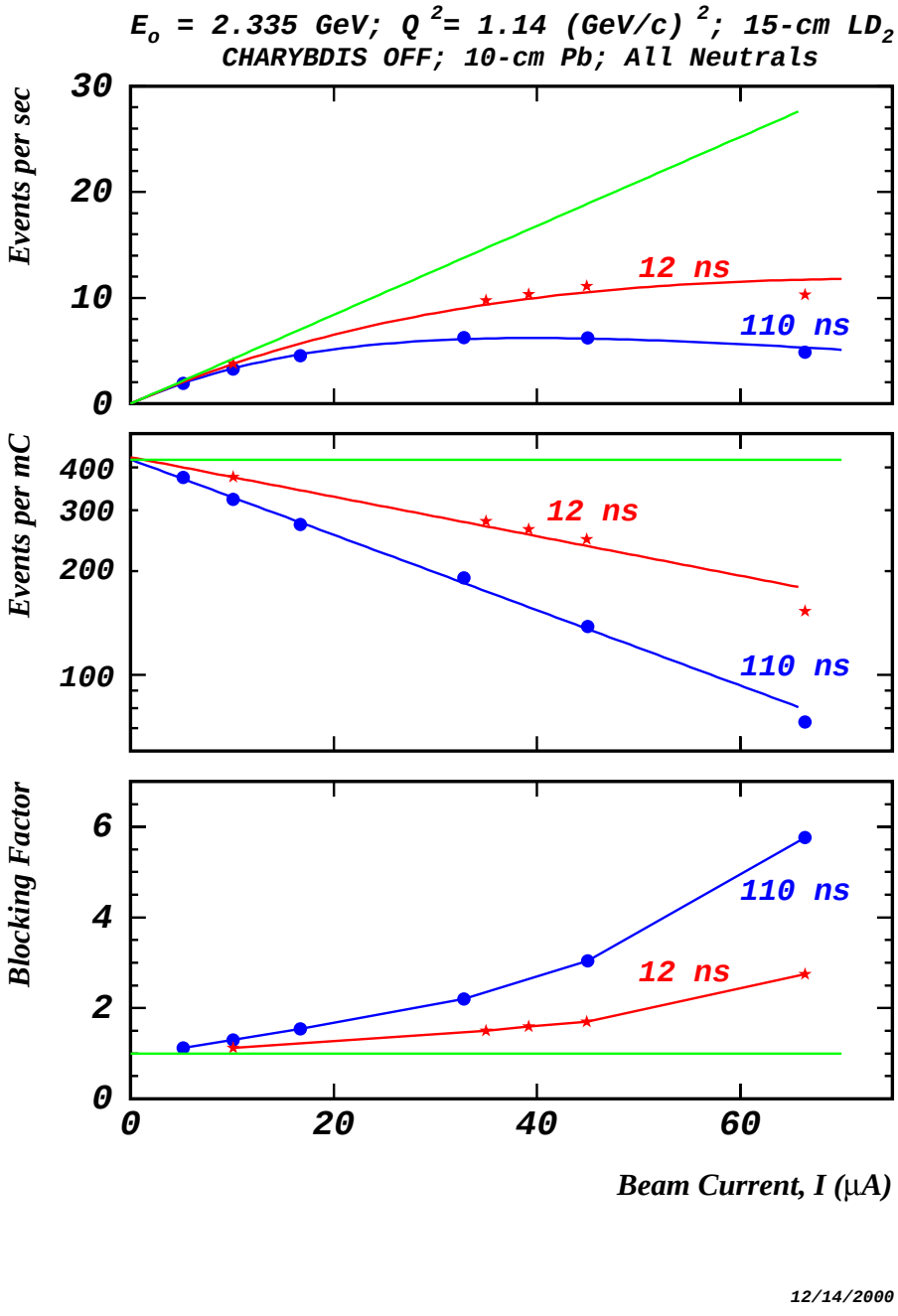

Figure 11: Event rate vs beam current at $Q^2 = 1.13$ (GeV/c)^2.

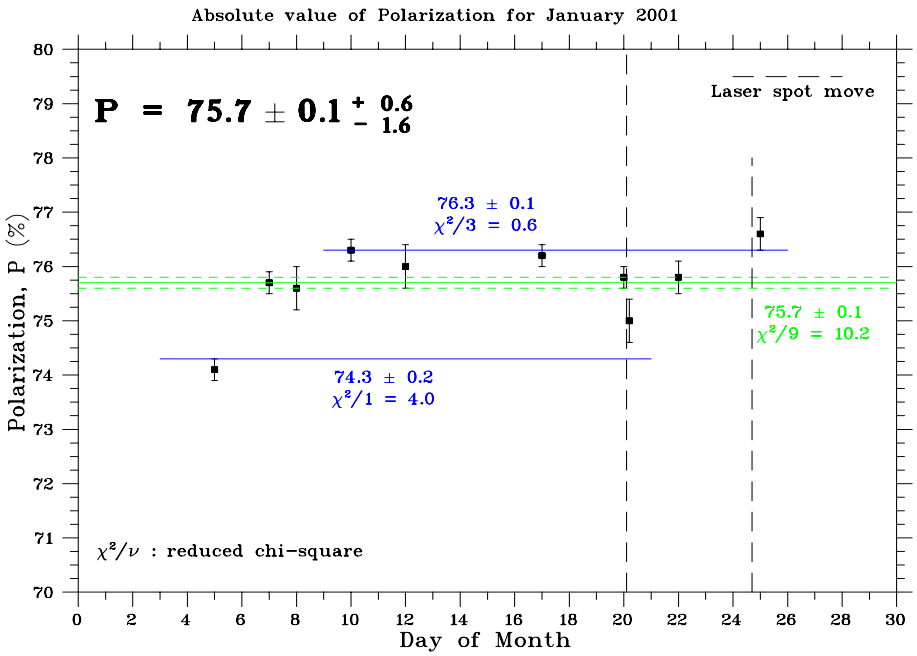

Figure 12: Electron beam polarization in January 2001.

ahead) from an estimate of the single rates in the HMS and the neutron polarimeter , and it can be expressed in terms of a measured blocking factor (BF):

$$CF(I) \;=\; \frac{BF(I)-1}{BF(I)} \tag{7}$$

where the blocking factor is

$$BF(I) \;=\; \frac{Rate(I)}{Rate(0)} \tag{8}$$

Here $Rate(I)$ is the number of events per mC of beam at beam current I, and $Rate(0)$ is the approximation of this value for $I = 0$. As shown in Fig. 11, a tight (12 ns) "software" window makes a substantial reduction in the blocking factor (i.e. fraction of corrupted events).

The absolute values of the beam polarization measured in January 2001 are plotted in Fig. 12.

2 Description of the Experiment

2.1 Experimental Arrangement

The experimental arrangement is shown in Fig. 13. A polarimeter detects the recoil neutron from the quasielastic d($\vec{e}$,e'$\vec{n}$)p reaction and measures up-down scattering asymmetry from the projection of the polarization vector on the transverse axis. A dipole magnet (CHARYBDIS) in front of the polarimeter precesses the neutron polarization vector through an angle χ to permit measuring the scattering asymmetry ξ_+ from the polarization vector component on the transverse (or sideways) direction. With another measurement of the scattering asymmetry ξ_-

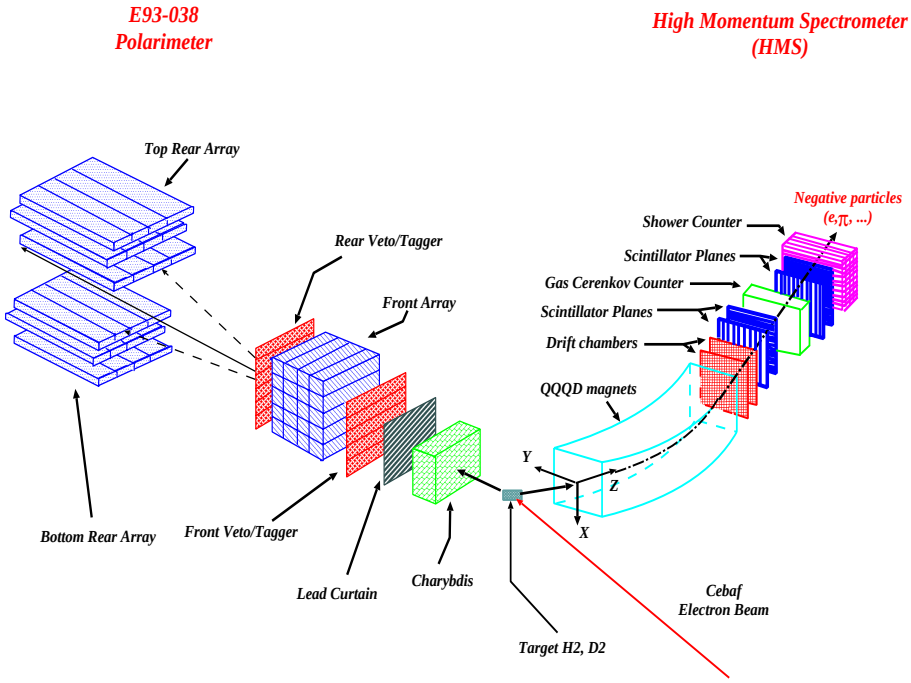

Figure 13: Schematic diagram of the experimantal arrangement.

for a precession through an angle $-\chi$, the ratio of G_E and G_M is given by

$$g \equiv \left(\frac{G_E}{G_M}\right) = K_R \, tan(\chi) \, \frac{(\eta+1)}{(\eta-1)} \tag{9}$$

where the asymmetry ratio

$$\eta \equiv \frac{\xi_-}{\xi_+} = \frac{P_-^x}{P_+^x} \tag{10}$$

and K_R is a kinematic function that is determined by the electron scattering angle θ_e in the d($\vec{e}$,e'$\vec{n}$)p reaction. For a total data-acquisition time T, the time fractions for measuring ξ_+ and ξ_- are optimized to minimize the statistical uncertainty in g. The scattered electron from the d($\vec{e}$,e'$\vec{n}$)p reaction is detected with the high-momentum spectrometer (HMS) in coincidence with the recoil neutron.

In E93-038, the polarimeter consisted of 20 detectors in the front array and 12 detectors in each of two rear arrays for a total of 44 detectors. A double layer of veto/tagger detectors is located ahead of the front array, and another double layer of tagger detectors is located behind the front array. This polarimeter was designed specifically for E93-038. To permit high luminosity, the dimensions of each of the 20 detectors in the front array were 10 cm×10 cm×100 cm, and the detectors in each rear array were shielded from the direct path of neutrons from the target. A prototype polarimeter with larger detectors in the front array was tested at Saturne with polarized neutrons of various energies. The analyzing powers and efficiencies extracted from the Saturne measurements permitted projections of rates and statistical uncertainties for E93-038, and this information is used here also.

The lead curtain ahead of the polarimeter is required to attenuate electromagnetic radiation and also to reduce the flux of charged particles incident on the polarimeter. The singles counting

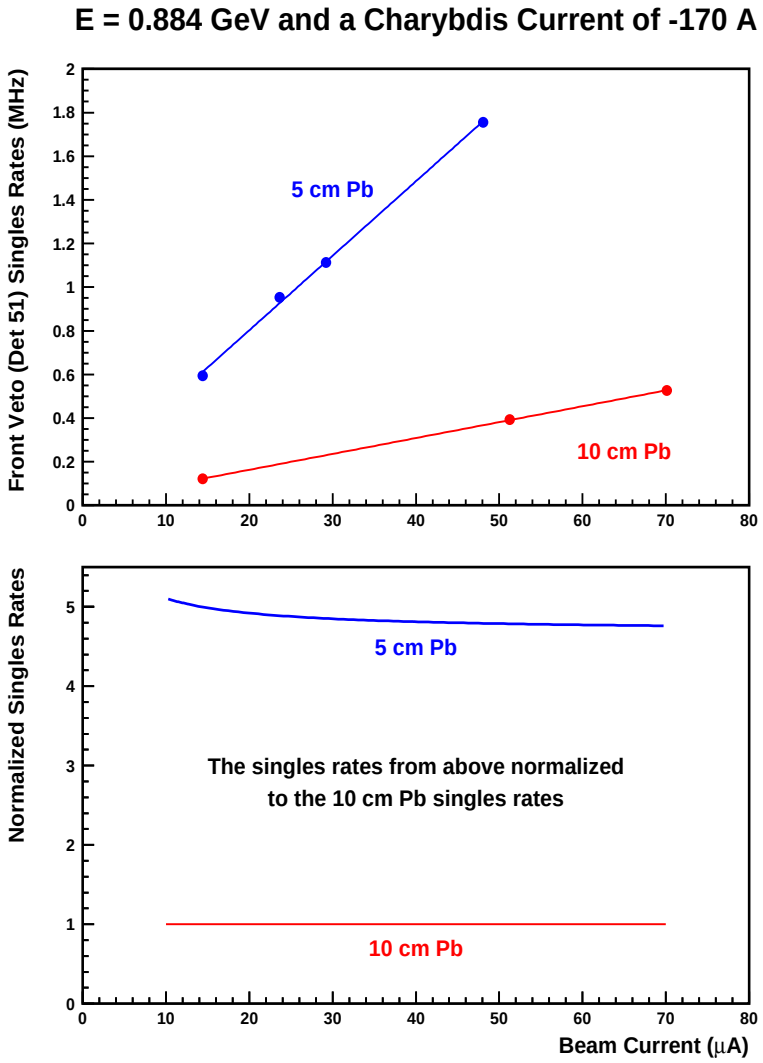

Figure 14: Singles rates for beam energy of 884 MeV and a CHARYBDIS current of -170 A.

rate in one of the detectors decreases markedly when the thickness of the Pb increases from 5 cm to 10 cm; for example, the singles rates in one of the veto detectors (160 cm wide × 11 cm high × 0.64 cm thick) at a distance of about 6.7 m from a 15-cm LD_2 target are plotted in Fig. 14 as a function of the electron beam current at an energy of 884 MeV. For all beam currents, the singles rate is about five times higher with 5-cm Pb curtain. E93-038 used a 10-cm lead curtain in order to run at higher beam currents. We do not have data with a 5-cm lead curtain at higher beam energies. E93-038 ran with a 10-cm Pb curtain for all these energies.

A significant advantage of this technique for measuring the ratio of the two scattering asymmetries is that the scale and systematic uncertainties are minimal because the relative uncertainty in the analyzing power of the polarimeter does not enter in the ratio. The same is true for the beam polarization because, as demonstrated in E93-038, P_L does not change much during sequential measurement of ξ_+ and ξ_-.

In the cross-ratio method of analysis of the scattering asymmetries measured in the polarimeter, Ohlsen and Keaton (1973) showed that false asymmetries cancel to all orders from

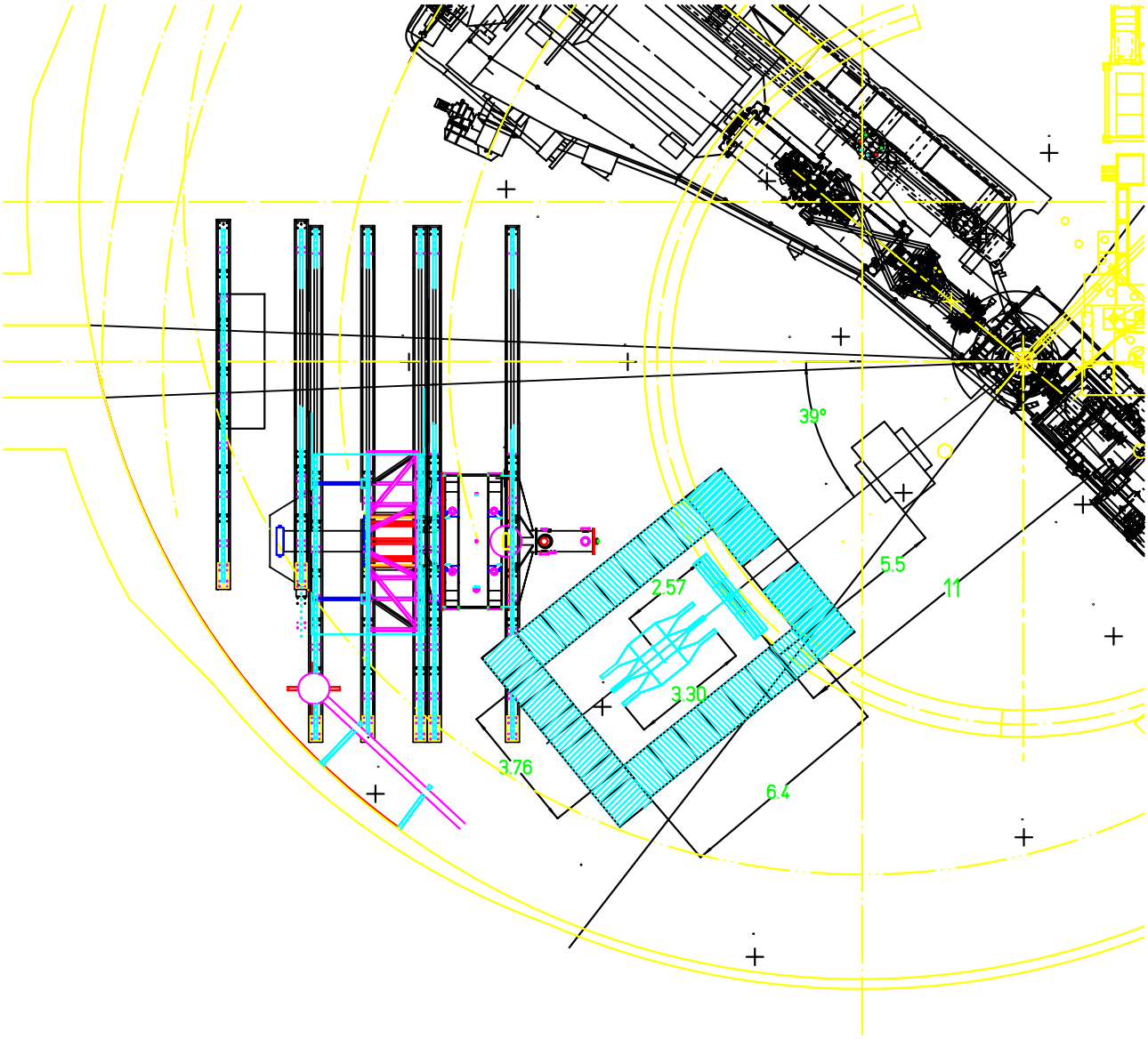

Figure 15: Footprint in Hall C of the polarimeter shielding enclosure for a neutron angle of 39 degrees and a mean flight path of 11.0 m. The shielding enclosure is compatible with the setup for the G_0 experiment by bridging over the floor rail for the G_0 magnet.

helicity-dependent errors in charge integration or system dead-times, or from errors in detection efficiency and acceptances; and that false asymmetries cancel to first order from misalingments with respect to $\vec{q}$, or from a difference in the beam polarization for the two helicity states. The cross ratio is the ratio of two geometric means $(N_U^+ N_D^-)^{1/2}$ and $(N_U^- N_D^+)^{1/2}$, where $N_U^+(N_D^-)$ is the yield in the peak for scattering neutrons up (down) when the helicity is positive (negative).

In E93-038, we used the CHARYBDIS dipole magnet with an 8.25-inch gap and 2-inch field clamps. The 8.25-inch gap is large enough to illuminate fully the front detector of our polarimeter (20-inch high by 40-inch wide). The precession angle χ is the angle of rotation of the polarization vector measured with respect to the direction of motion of the particle in the rest frame of the particle after traversing the magnetic field. The neutron spin precession angle χ is given by

$$\chi \;=\; -\frac{ge}{2M_p c\beta_n} \int B\Delta l \;=\; \frac{1.913e}{M_p c\beta_n} \int B\Delta l \tag{11}$$

where $g/2$ = -1.913. The maximum central $\int B\Delta l$ = 2.39 Tm for CHARYBDIS with an 8.25-inch gap.

Figure 15 is a footprint in Hall C of the polarimeter shielding enclosure for a neutron angle of 39 degrees and a mean flight path of 11.0 m to the mid-plane of the front detector array in the polarimeter. This setup is compatible with the setup for the G_0 experiment.

2.2 Kinematics

Four-Momentum Transfer, Q^2 (GeV/c)^2	1.69	2.08	2.40
Beam Energy, E_0 (GeV)	2.558	3.395	4.232
Electron Scattering Angle, θ_e (deg)	36.71	29.97	25.29
Scattering Electron Momentum, P_e' (GeV/c)	1.661	2.289	2.956
Neutron Scattering Angle, θ_n (deg)	39.0	39.0	39.0
Neutron Momentum, P_n (GeV/c)	1.578	1.817	2.007
Neutron Kinetic Energy, T_n (MeV)	897	1106	1276
Neutron Velocity, β_n	0.859	0.888	0.906
Flight Path, x (m)	11.0	11.0	11.0
Neutron Energy Resolution (HWHM), ΔT_n (MeV)	46	67	87
Field Integral to Precess Neutron Spin through 40 Degree, $B\Delta l$ (Tm)	0.9820	1.0152	1.0351
CHARYBDIS Current, I (A)	243.45	251.65	256.56

Table 1: Kinematic conditions at a neutron scattering angle of 39^o and a beam energy per pass of 837 MeV. Also listed are the neutron energy resolution and the Charybdis field integral $B\Delta l$ required to precess the neutron polarization vector through $\pm$ 40 degrees. Quantities are listed also for Q^2 = 1.69 and 2.08 (GeV/c)^2 because these two points could be obtained with a three-pass and a four-pass beam, respectively.

Table 1 lists the kinematics conditions, the $B\Delta l$ required to precess the neutron polarization vector through $\pm$ 40 degrees, and the neutron energy resolution at a mean flight path of 11.0 m.

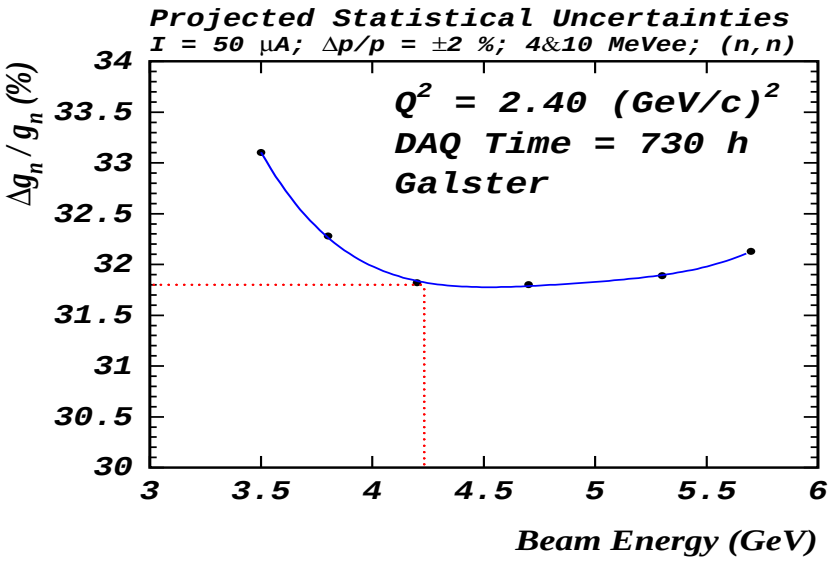

Figure 16: Statistical uncertainty, projected at $Q^2 = 2.4$ (GeV/c)^2, as a function of beam energy.

The neutron energy resolution is sufficient to discriminate against neutrons associated with pion production.

The beam energy per pass of 837 MeV was selected because it was used in E93-038 and gave a high beam polarization. Also for $Q^2 = 2.4$ (GeV/c)^2, the five-pass beam energy of 4.232 GeV is in a region where the accelerator operates reliably, and this beam energy results in a minimum or near-minimum statistical uncertainty, as seen in Fig. 16, for the Galster parameterization of G_E^n.

The range of reasonable angles of neutron spin precession is limited on the small-angle side by the requirement to have the magnetic field in CHARYBDIS strong enough to deflect the quasielastic protons away from the front array of the polarimeter, and on the large-angle side by the fact that the statistical uncertainty $\Delta g_n/g_n$ increases with precession angle χ, as shown in Fig. 17. The precession angle χ of 40^o was chosen.

2.3 Count Rates

The rate of electron-neutron coincidence events, which comes from quasielastic scattering of electrons on the 15-cm LD_2 target, was projected for a beam current of 50 μA (which corresponds to a beam luminosity $L = 2.39 \times 10^{38} cm^{-2} s^{-1}$). The calculation was done for a momentum bite $\Delta p/p$ of $\pm\, 2.0\%$ for the scattered electron. This restricted HMS momentum bite helps to suppress the "false asymmetry" neutrons from the two-step process d($\vec{e}$,e'$\vec{p}$)n + Pb($\vec{p}$,$\vec{n}$). Protons that originate from quasielastic scattering at the angle of 39^o will be deflected away from the front array of the polarimeter by the magnetic field of Charybdis. In exchange for these protons, the protons emitted from the target at another angle (and corresponding to another value of Q^2 and a "shifted" value of the momentum of the scattered electrons) will be deflected into the front array. This effect was observed in E93-038 (see Fig. 18), and application of a tight cut on

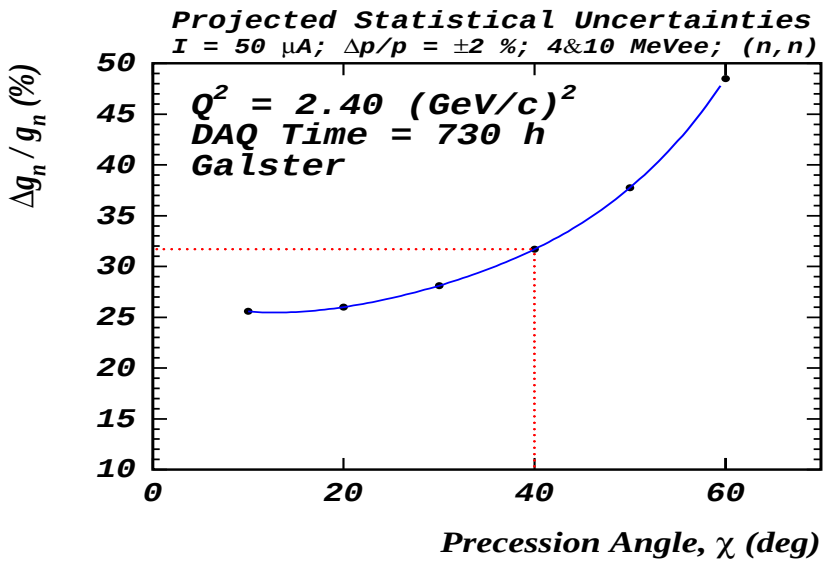

Figure 17: Statistical uncertainty, projected at $Q^2 = 2.4$ (GeV/c)^2, as a function of precession angle.

the momentum of the electron in HMS reduces the "false asymmetry" effect significantly. Also the restricted HMS momentum bite helps to suppress the neutrons associated with the pion production.

The acceptances for E93-038 were calculated for the HMS in the normal-quad mode and in the rear position. We used the kinematic conditions from Table 1 for the Q^2-point of 2.4 (GeV/c)^2. Based on the acceptance-averaged coincidence rate $< R_{MCEEP} >$ from MCEEP by Ulmer (1991) [version 3.1, which includes radiative corrections], we estimated the real-event rate R_{real} for a neutron transmission $t = 0.57$ [through a 10-cm Pb curtain], an HMS efficiency $\epsilon_{HMS} = 0.92$ [which is the product of a single-hit fraction in the wire chambers (0.95) and an efficiency for tracking a good electron (0.97)], and a live-time fraction of the data-acquisition system of 0.95. We used a value of 0.0040 as an estimate of the neutron polarimeter efficiency value for software thresholds of 4 (10) MeV on the front (rear) detector. This value is an extrapolation of the results of polarimeter efficiency measurements at Saturne (France, 1996) for neutrons up to 1057 MeV; these measurements were corrected for the E93-038 rear-array geometry. Listed in Table 2 are neutron polarimeter and HMS acceptances, estimated neutron polarimeter parameters (viz., A_Y and ϵ_n), and the calculated real event rate.

2.4 Projected Uncertainties

The top-bottom asymmetry, measured in JLab E93-038 experiment, is proportional to the projection of the neutron polarization vector on the axis that is perpendicular to the neutron momentum direction. So, the ratio of asymmetries for neutron spin precession through $\pm\chi$ degrees:

$$\eta \equiv \frac{\xi_-}{\xi_+} = \frac{P_-^x}{P_+^x} = \frac{P_{S'}cos(-\chi) + P_{L'}sin(-\chi)}{P_{S'}\ cos(\chi) + P_{L'}\ sin(\chi)} = \frac{(P_{S'}/P_{L'})\ cos(\chi) - sin(\chi)}{(P_{S'}/P_{L'})\ cos(\chi) + sin(\chi)} \qquad (12)$$

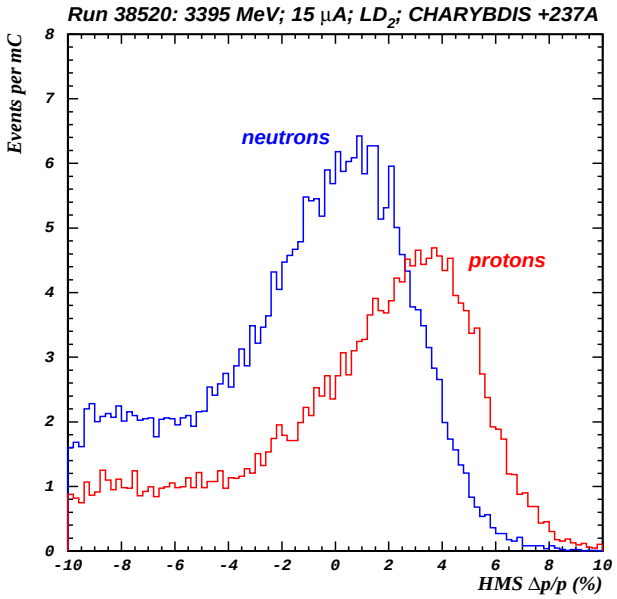

Figure 18: Momentum distributions for electrons in HMS associated with the neutrons and protons scattered into the polarimeter.

$$(P_{S'}/P_{L'}) = \frac{-sin(\chi)\ (\eta+1)}{cos(\chi)\ (\eta-1)} = -tan(40^o)\ \frac{(\eta+1)}{(\eta-1)} \tag{13}$$

where $P_{S'}$ and $P_{L'}$ are transverse and longitudinal projections of the neutron polarization vector:

$$P_{S'} \ = \ -h\ P_e\ \frac{K_S\ g}{K_0\ (1\ +\ g^2/K_0)} \tag{14}$$

$$P_{L'} \ = \ h\ P_e\ \frac{K_L}{K_0\ (1\ +\ g^2/K_0)} \tag{15}$$

Here h is the beam helicity, P_e is the beam polarization, and $g \equiv (G_E/G_M)$.

$$(P_{S'}/P_{L'}) \ = \ -g\ (K_S/K_L) \tag{16}$$

From (14) and (11) :

$$g \ = \ -\left(\frac{K_L}{K_S}\right)\ \left(\frac{P_{S'}}{P_{L'}}\right) \ = \ \left(\frac{K_L}{K_S}\right)\ tan(\chi)\ \frac{(\eta+1)}{(\eta-1)} \tag{17}$$

The statistical uncertainty in the g value is:

$$(\delta g)_{stat} \ = \ \left(\frac{K_L}{K_S}\right)\ tan(\chi)\ \frac{2}{(\eta-1)^2}\ \delta\eta \tag{18}$$

The relative statistical uncertainty $(\delta g/g)_{stat}$ is:

$$\left(\frac{\delta g}{g}\right)_{stat} \ = \ \frac{2}{(\eta+1)(\eta-1)}\ \delta\eta \tag{19}$$

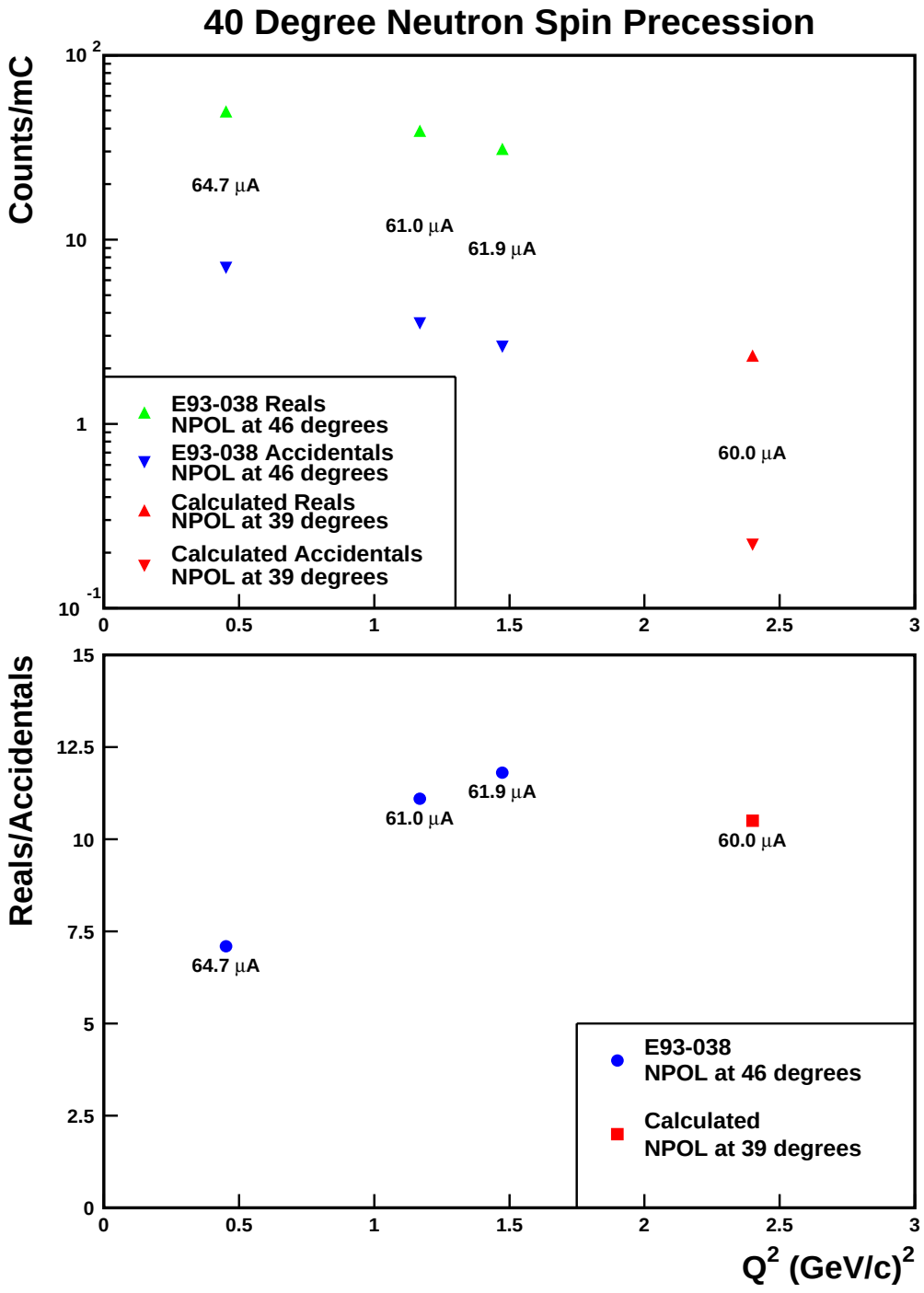

Figure 19: Real event rate, accidental coincidence rate, and the reals-to-accidentals ratio obtained from E93-038 and from a calculation at $Q^2 = 2.4$ (GeV/c)^2.

HMS angular acceptance:	
$\Delta\theta_e$ (mrad)	$\pm$ 27.5
$\Delta\phi_e$ (mrad)	$\pm$ 71.9
Neutron polarimeter angular acceptance:	
$\Delta\theta_n$ (mrad)	$\pm$ 45.4
$\Delta\phi_n$ (mrad)	$\pm$ 22.7
Neutron polarimeter efficiency, ϵ_n (%)	0.40
MCEEP rate, $< R_{MCEEP} >$ (Hz)	41.2
Real-event rate, R_{real} (Hz)	0.12
Neutron polarimeter analyzing power, A_Y	0.160

Table 2: The neutron polarimeter and HMS acceptances, estimated neutron polarimeter parameters, and calculated real event rate at $Q^2 = 2.4$ (GeV/c)^2.

Here $\delta\eta$ is the statistical error in the asymmetry ratio:

$$\left(\frac{\delta\eta}{\eta}\right)^2 \;=\; \left(\frac{\delta\xi_-}{\xi_-}\right)^2 \;+\; \left(\frac{\delta\xi_+}{\xi_+}\right)^2 \tag{20}$$

or

$$(\delta\eta)^2 \;=\; \left(\frac{\delta\xi_-}{\xi_+}\right)^2 \;+\; \xi_-^2\left(\frac{\delta\xi_+}{\xi_+^2}\right)^2 \tag{21}$$

To project the statistical uncertainties, we used the statistical errors for asymmetries which come from Poisson statistics:

$$\left(\frac{\delta\xi_\pm}{\xi_\pm}\right)^2 \;=\; \frac{1}{\xi_\pm^2}\left(\frac{1+2/r}{N_\pm}\right) \;=\; \frac{1}{(A_Y P_\pm^x)^2}\left(\frac{1+2/r}{N_\pm}\right) \tag{22}$$

Here $N_\pm$ is the number of events taken during $\pm\, 40^o$ precession angle runs, A_Y is the polarimeter analyzing power, and r is the ratio of real-to-accidental coincidences. For these projections, the value $r = 6$. Values of r achieved in E93-038 are plotted in Fig. 19 as a function of Q^2.

The projected uncertainty $\Delta g_n/g_n$ is plotted in Fig. 20 as a function of the data acquisition time for a luminosity of 2.39×10^{38} cm^{-2}s^{-1}, which is achievable with a beam current of 50 μA on a 15-cm liquid deuterium target. The DAQ times that are designated by dotted lines in Fig. 20 were chosen to yield an uncertainty $\Delta G_E^n = 0.0045$. Projected statistical uncertainties in G_E^n with $\Delta G_M^n/G_M^n = 0.050$ are plotted in Fig. 21 as a function of data acquisition time. Recent Hall B measurements of G_M^n up to $Q^2 = 4.8$ (GeV/c)^2 [Brooks et al. (1994)], which are being analyzed currently, should reduce the relative uncertainties in G_M^n.

2.5 Another Polarization-Transfer Technique to Measure G_E^p/G_M^p

We describe here the possibility of carrying out an *incidental* measurement of g_p [$\equiv G_E^p/G_M^p$] by another independent polarization-transfer technique for the purpose of determining if there is a fundamental problem with either the Rosenbluth or focal-plane polarimeter (FPP) methods.

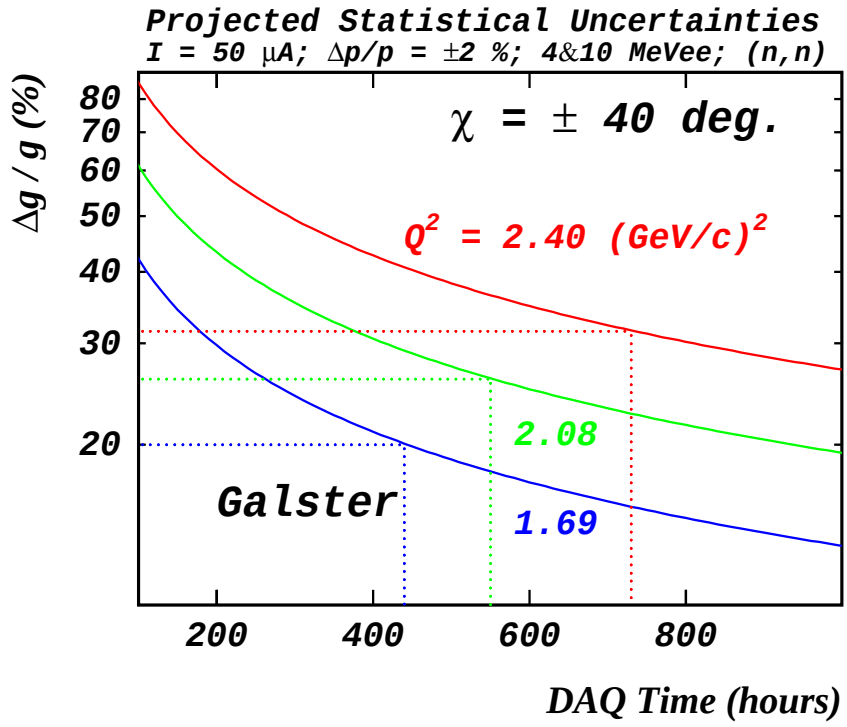

Figure 20: Projected uncertainty $\Delta g_n/g_n$ as a function of the DAQ time. The beam current is 50 μA, and the corrupted fraction (see text) is 15%.

Our proposed measurement of G_E^p would be incidental to the G_E^n measurement. With a relatively small investment of time, the g_p measurement at $Q^2 = 2.08$ (GeV/c)^2 is designed to distinguish clearly between $\mu_p g_p = 0.73$ from JLab E93-027 and $\mu_p g_p \approx 1$ from the SLAC global analysis.

JLab experiment 93-027 ran successfully during summer 1998 and measured G_E^p/G_M^p for Q^2 between 0.5 and 3.5 (GeV/c)^2. As reported by Jones at al. (2000), the result for the ratio G_E^p/G_M^p revealed a systematic decrease with increasing Q^2, as shown in Fig. 3. This surprising result indicated for the first time a marked difference in the spatial distribution of charge and magnetization currents in the proton. These measurements were made with the focal plane polarimeter (FPP) in Hall A, and were extended to 5.6 (GeV/c)^2 in E99-007. The E99-007 collaboration found that the systematic decrease in $\mu_p G_E^p/G_M^p$ continued to 5.6 (GeV/c)^2. Now a new proposal has been submitted to PAC 20 to extend these measurements to 9 (GeV/c)^2 with a new focal-plane polarimeter (FPP) in the high momentum spectrometer in Hall C. Because the JLab measurements via the (FPP) polarization-transfer technique disagree with prior SLAC measurements via the Rosenbluth separation technique, PAC 19 approved a new measurement of G_E/G_M for the proton (E01-001). This new measurement uses a modified Rosenbluth separation technique that promises smaller uncertainties. The PAC 19 report states that "It is of great importance to determine if there is a fundamental problem with either the Rosenbluth or polarization-transfer methods, as they are also used for many other experiments." As shown in Fig. 22, the dependence in the values of μg_p between the Hall A and SLAC data increases with Q^2.

The E93-038 collaboration demonstrated the ability to measure $g_p \equiv (G_E^p/G_M^p)$ by another

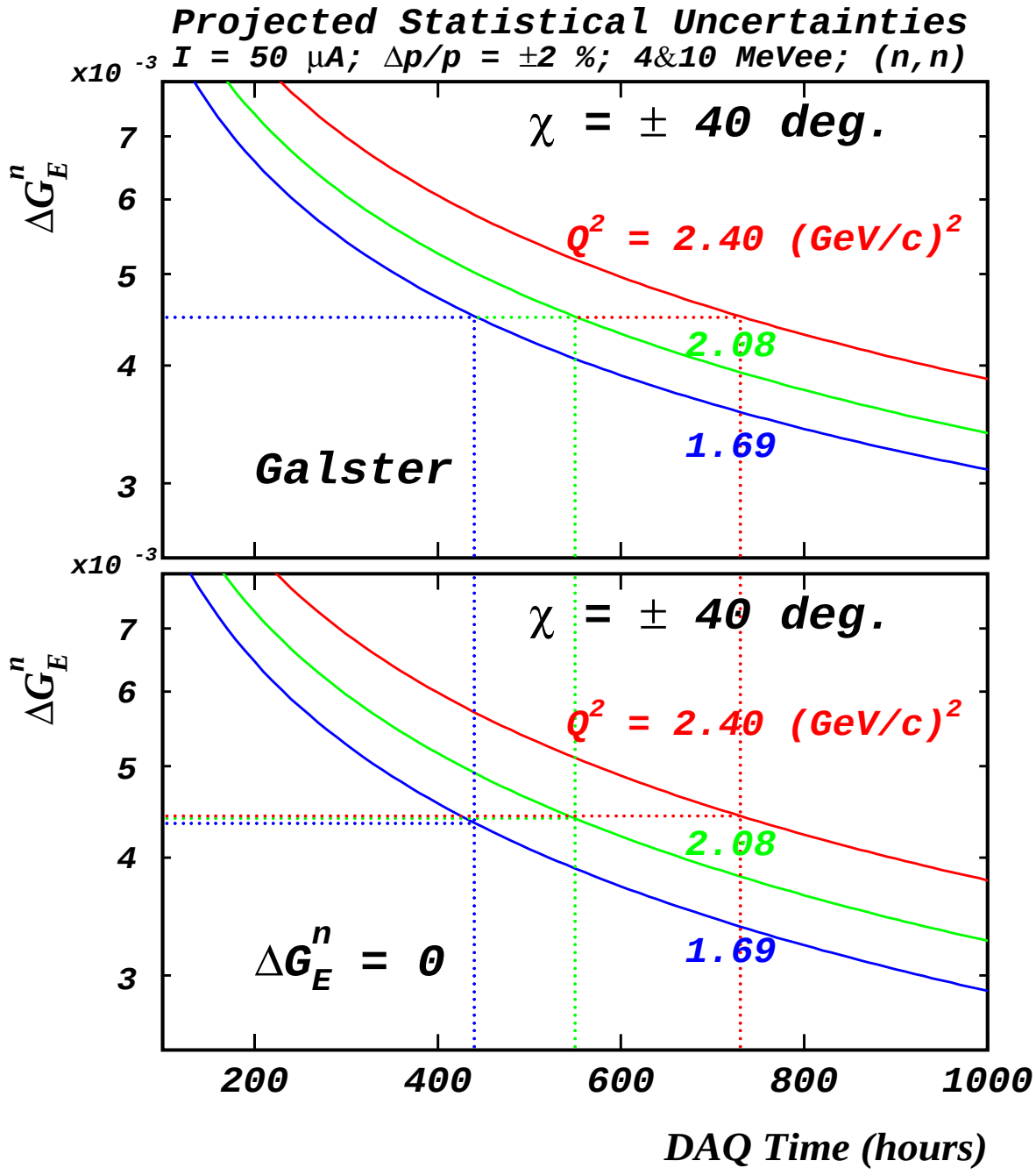

Figure 21: Projected uncertainty G_E^n as a function of the DAQ time for Galster parameterization and $G_E^n = 0$. The beam current is 50 μA, and the corrupted fraction (see text) is 15%.

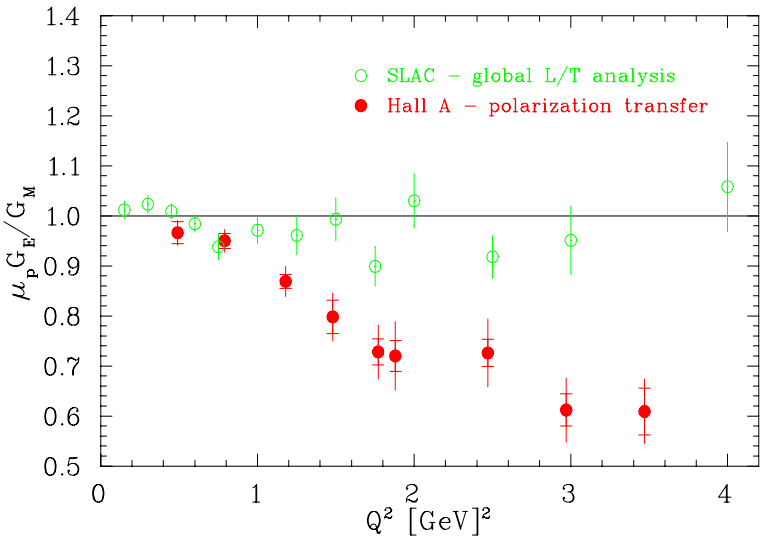

Figure 22: $\mu_p g_p$ as a function of Q^2.

polarization-transfer technique, which makes use of a dipole magnet ahead of a polarimeter. An initial zeroth-order analysis of the data at $Q^2 = 1.13$ (GeV/c)^2 yielded a very preliminary result for g_p (with a statistical uncertainty of about 8% in $\approx$ 24 hours of beam time at an average beam current of 70 μA) that is consistent with the dipole value and with the value reported by Jones et al. (2000) at $Q^2 = 1.18$ (GeV/c)^2. It is necessary to make a measurement at a higher value of Q^2 where the measurements of Jones at al. (2000) fall clearly below the dipole value; accordingly, we propose to measure $\mu_p g_p$ at $Q^2 = 2.08$ (GeV/c)^2 (with a statistical uncertainty of $\approx$ 10% and a significantly smaller systematic uncertainty). Jones et al. (2000) found $\mu_p g_p = 0.720 \pm 0.031 \pm 0.060$ at $Q^2 = 1.88$ (GeV/c)^2 and $\mu_p g_p = 0.726 \pm 0.027 \pm 0.062$ at Q^2 = 2.47 (GeV/c)^2. [Note that the systematic uncertainties in the FPP measurements are larger ($\approx$ 8%) because of the uncertainty in the precession through the spectrometer]. The statistical uncertainty of 10% is sufficient to distinguish clearly between $\mu_p g_p = 0.73$ from JLab E93-027 and $\mu_p g_p \approx 1$ from the SLAC global analysis.

The method proposed here with a dipole precession magnet and a stand-alone proton polarimeter has the advantage over the FPP method that the precession of the polarization vector is easy to calculate and practically no error can occur. A drawback of this method is that the precession angle χ is small, and the error diverges as $1/\chi$; however, this technique has the capability of distinquishing between the results from JLab and those from SLAC without requiring substantial beam time. The statistical uncertainty $\Delta g_p/g_p$ was projected using electron-proton coincidence event rate from MCEEP program by Ulmer (1991). This uncertainty is plotted in Fig. 23 as a function of DAQ time; for $\Delta g_p/g_p = 0.10$, the beam time is 50 hours ($\approx$ 2 days) with a 70 μA beam on a 15-cm LH_2 target.

3 Beam Time

We estimate that 730 hours of acquisition time for "good" (not junk) runs on a 15-cm LD_2 target will be needed to produce a statistical uncertainty $\Delta G_E^n = 0.0045$ at $Q^2 = 2.40$ (GeV/c)^2.

	Hours	Days
Commissioning without beam		
Pulse-height calibration and cosmic-ray tests	168	7
Commissioning with beam		
HMS	24	1
Moeller Polarimeter	24	1
NPOL (check detectors, adjust timing, adjust thresholds, adjust Pb curtain thickness, determine optimum beam current, etc.)	48	2
Total commisioning with beam	**96**	**4**
G_E^n physics measurements		
LD_2 target	730	30.4
LH_2 target	96	4
Dummy target	72	3
Beam polarization	72	3
Time calibrations	48	2
Overhead[(a)]	72	3
Total G_E^n physics measurements	**1090**	**45.4**
Total beam time for G_E^n at $Q^2 = 2.40$ (GeV/c)^2	**1186**	**49.4**
G_E^p measurements commissioning (determine correct CHARYBDIS current, determine optimum beam current)	16	0.67
G_E^p physics measurements		
LH_2 target	50	
Dummy target	6	
Beam polarization	4	
Time calibrations	4	
Overhead[(b)]	6	
Total G_E^p physics measurements	**70**	**2.92**
Total beam time for G_E^p at $Q^2 = 2.08$ (GeV/c)^2	**86**	**3.6**
Total $G_E^n + G_E^p$ measurements	**1272**	**53**

Table 3: Beam-time request for measuring G_E^n at $Q^2 = 2.40$ (GeV/c)^2 for a 50 μA, 70% polarized beam on a 15-cm LD_2 target, and an incidental measurement of G_E^p at $Q^2 = 2.08$ (GeV/c)^2 for a 70 μA, 70% polarized beam on a 15-cm LH_2 target.

(a) 115 changes in Charybdis dipole current, 69 target changes, starting and stopping the DAQ system at least 1012 times for runs that are typically 2 hours long.

(b) One beam energy change, 19 changes in Charybdis dipole current, 4 target changes, starting and stopping the DAQ system at least 28 times.

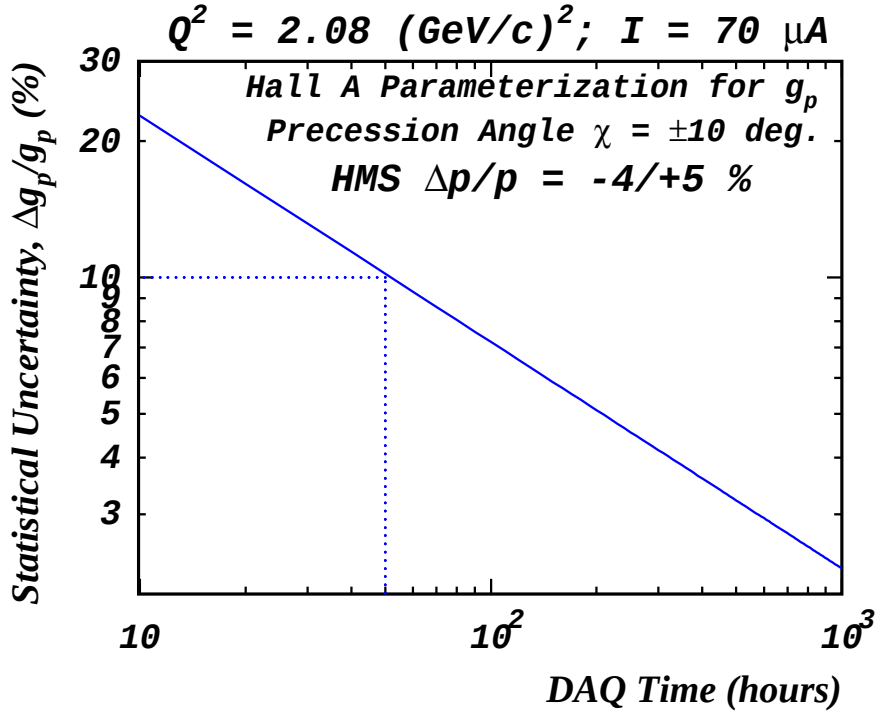

Figure 23: Projected statistical uncertainty $\Delta g_p/g_p$ as a function of the DAQ time.

These 730 hours will require a beam polarization of 70 percent at a current of 50 μA on a 15-cm LD_2 target. The projection was based on a calculation of a fraction of electron-neutron coincidence events corrupted from a background particle (charged or neutral) that appears during the coincidence time window (see Fig. 24). For a 50 μA beam, the corrupted fraction is calculated to be 15%.

The relevant beam time that determines the statistical uncertainty at each data point is the sum of times calculated for each run as the ratio of the accumulated charge to the beam current for each "good" (not junk) run with LD_2, LH_2, and dummy targets. A correction for runs with the Moeller target is small. In E93-038, the relevant beam time calculated in this straightforward manner revealed that E93-038 logged 33.2 days out of a total of 88 days scheduled at 2.332 and 3.395 GeV for a statistically-relevant beam utilization of 37.7%. This 37.7% factor does not include overhead time [totalling $\approx$ 25%] for such items as target changes, changing the current in CHARYBDIS dipole magnet, starting and stopping the DAQ, recovery from short-term beam trips and HMS trips (unless reported by shift chiefs), and runs with "bad data". This 37.7% factor is lower than that obtained from the reports of Acceptable Beam in Use [ABU], which report 50.6% at 2.332 GeV and 51.0% at 3.395 GeV. The difference between the utilization based on ABU's and that based on $Q_{total}/ < I >$ can be understood; the two numbers are commensurate when we account for the fact that the beam-on time that generates "good data" is about 75% of the ABU time. *An ABU percentage of 50% is marginal* for achieving projected statistics unless the projected time includes a factor of about 4/3; without this factor, an ABU percentage of $\approx$ 66% is needed. It is our understanding that the downtime reflected in the ABU's includes only accelerator and Hall C equipment downtime, and that it does not

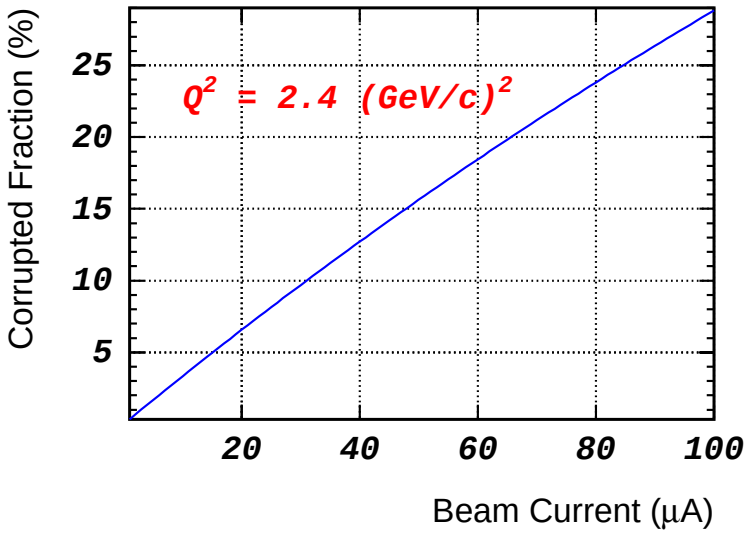

Figure 24: Calculated fraction of electron-neutron coincidence events corrupted from a background particle (charged or neutral) that appears during the coincidence time window of 70 ns as a function of the beam current.

include the items of experimental overhead mentioned above. Our beam-time request includes an explicit amount (**not the 4/3 factor**) for such experimental overhead [see footnote (a) to Table 3].

Our beam-time request for measuring G_E^n at $Q^2 = 2.40$ (GeV/c)^2 is shown in Table 3. Also shown in Table 3 is the additional time to make an incidental measurement of G_E^p at $Q^2 = 2.08$ (GeV/c)^2.

The proposed measurements can be done also in Hall A. It turns out that the counting rates are essentially the same. This collaboration is willing to run in Hall A if the experiment can be scheduled earlier in Hall A than in Hall C.

4 Collaboration

Each of the participants listed earlier contributed to the success of E93-038. The collaboration is a strong, experienced, and large team (currently about 71 scientists from 22 institutions). Graduate students will be added after the proposed experiment is approved and scheduled.

As in E93-038, Kent State University (KSU) will be responsible for the neutron polarimeter; MIT, for CHARYBDIS; and JLab for the HMS. KSU provided the neutron detectors in the rear array and the polarimeter electronics; Hampton University provided one-half of the neutron detectors in the front array, while JLab provided the other half. The University of Virginia provided the tagger detectors used in E93-038. Duke University took responsibility for the Analysis Engine and also for setting up the electronics and timing. Professor James J. Kelly at the University of Maryland spearheaded the development of the analysis programs used in E93-038, and Dr. A.Yu. Semenov is the czar of the E93-038 analysis effort. T. Reichelt (Bonn),

H. Fenker (JLab), and S. Danagoulian (NCAT) were the lead scientists in establishing the operating conditions for running the Moeller polarimeter at a beam energy below one GeV, and in setting up and running the Moeller polarimeter at the two higher energies. A. Ahmidouch (NCAT) and S. Taylor (MIT) were the lead scientists in mapping the CHARYBDIS dipole magnet. A. Ahmidouch (NCAT) was the lead scientist in preparing the run plan to obtain data for new matrix elements for the HMS. For this proposal, the personnel at the same institutions will provide their expertise. With respect to equipment, we anticipate the need for a few additional 10-in $\times$ 40-in $\times$ 4-in neutron detectors in order to replace the 20-in $\times$ 40-in $\times$ 4-in detectors in the rear array. Kent State U did not have quite enough to replace each 20-in $\times$ 40-in $\times$ 4-in detector with two 10-in $\times$ 40-in $\times$ 4-in detectors in E93-038.

References

[Arenhoevel 1987] H. Arenhoevel, Phys. Lett. **B199**, 13 (1987).

[Arenhoevel 1988] H. Arenhoevel *et al.*, Z. Phys. **A331**, 123 (1988).

[Aznaurian 1993] I.G. Aznaurian, Phys. Lett. **B316**, 391 (1993).

[Beck 1992] G. Beck and H. Arenhoevel, Few Body Systems **13**, 165 (1992).

[Cardarelli 2000] F. Cardarelli, S. Simula, Phys. Rev. **C62**, 065201 (2000).

[Chung 1991] P.L. Chung and F. Coester, Phys. Rev. **D44**, 229 (1991).

[Dong 1998] S.J. Dong, K.F. Liu, and A.G. Williams, Phys. Rev. **D58**, 074504 (1998).

[Eden 1994] T. Eden *et al.*, Phys. Rev. **C50**, R1749 (1994).

[Feshbach 1967] H. Feshbach and E. Lomon, Rev. Mod. Phys. **39**, 611 (1967).

[Frank 1996] M.R. Frank, B.K. Jennings, and G.A. Miller, Phys. Rev. **C54**, 920 (1996).

[Friar 1990] J.L. Friar, Phys. Rev. **C42**, 2310 (1990).

[Gari 1985] M.F. Gari and W. Krumpelmann, Z. Phys. **A322**, 689 (1985).

[Gari 1992] M.F. Gari and W. Krumpelmann, Phys. Lett. **B274**, 159 (1992).

[Galster 1971] S. Galster, H. Klein, J. Moritz, K.H. Schmidt, D. Wegener, and J. Blechwenn, Nucl. Phys. **B32**, 221 (1971).

[Herberg 1999] C. Herberg *et al.*, Eur. Phys. J. **A5**, 131 (1999).

[Holzwarth 1996] G. Holzwarth, Z. Phys. **A356**, 339 (1996).

[Isgur 1998] N. Isgur, Phys. Rev. Lett. **83**, 272 (1999).

[Isgur 2000] N. Isgur and J.W. Negele, Nuclear Theory with Lattice QCD, a proposal to DOE, PI's (2000).

[Jones 2000] M. Jones *et al.*, Phys. Rev. Lett. **84**, 1398 (2000).

[Kelly 2001] J.J. Kelly, Time Calibration Procedures for E93-038 Polarimeter: Version 2.2, JLab E93-038 internal report (2001),
URL: *http://www.physics.umd.edu/enp/e93038/time_calibration.ps*

[Klein 1997a] F. Klein and H. Schmieden, Nucl. Phys. **A623**, 323c (1997).

[Klein 1997b] F. Klein, Proc. of the 14th Int. Conf. on Particles and Nuclei, ed. by C.E. Carlson and J.J. Domingo, World Scientific 1997, p.121.

[Kroll 1992] P. Kroll, M. Schurmann, and W. Schweiger, Z. Phys. **A342**, 429 (1992).

[Laget 1990] J.M. Laget, Phys. Lett. **B273**, 367 (1990).

[Liu 2001] K.F. Liu, Private Communication (2001).

[Lu 1998] D.H. Lu, A.W. Thomas, and A.G. Williams, Phys. Rev. **C57**, 2628 (1998).

[Lung 1993] A. Lung *et al.*, Phys. Rev. Lett. **70**, 718 (1993).

[Mergell 1996] P. Mergell, U.G. Meissner, D. Drechsel , Nucl. Phys. **A596**, 367 (1996).

[Meyerhoff 1994] M. Meyerhoff *et al.*, Phys. Lett. **B327**, 201 (1994).

[Mosconi 1991] B. Mosconi, J. Pauchenwein, and P. Ricci, Proceedings of the XIII European Conference on Few-Body Problems in Physics, Marciana Marina (Elba), Italy (September 1991).

[Ohlsen 1973] G.G. Ohlsen and P.W. Keaton, Jr., Nucl. Instr. Meth. **109**, 41 (1973).

[Ostrick 1994] M. Ostrick *et al.*, Phys. Rev. Lett. **83**, 276 (1999).

[Pace 2000] E. Pace, G. Salme, F. Cardarelli, and S. Simula, Nucl. Phys. **A666**, 33 (2000).

[Passchier 1999] I. Passchier *et al.*, Phys. Rev. Lett. **82**, 4988 (1999).

[Platchkov 1990] S. Platchkov *et al.*, Nucl. Phys. **A508**, 343c (1990).

[Radyushkin 1984] A.V. Radyushkin, Acta Phys. Polon. **B15**, 403 (1984).

[Rekalo 1989] M.P. Rekalo, G.I. Gakh, and A.P. Rekalo, J. Phys. **G15**, 1223 (1989).

[Rohe 1999] D. Rohe *et al.*, Phys. Rev. Lett. **83**, 4257 (1999).

[De Sanctis 2000] M. De Sanctis, M.M. Giannini, L. Repetto, and E. Santopinto, Phys. Rev. **C62**, 025208 (2000).

[Schmieden 1996] H. Schmieden, Proc. of the 12th Int. Symposium on High-Energy Spin Physics, Amsterdam (1996), ed. by C.W. de Jager et al., World Scientific 1997, p.538.

[Ulmer 1991] P.E. Ulmer, MCEEP – Monte Carlo for Electro-Nuclear Coincidence Experiments, CEBAF–TN–91–101 (1991).

[Zhu 2001] H. Zhu *et al.*, A Measurement of the Electric Form-Factor of the Neutron through $\vec{d}(\vec{e}, e'n)p$ at $Q^2 = 0.5$ (GeV/c)^2, e-print **nucl-ex/0105001** (2001).